이학박사 학위논문

Pivotal functional roles of Neuropilin-2 in cell motility and invasion in head and neck squamous cell carcinoma

두경부 편평상피세포암에서 세포 이동성과

침습능에 대한 Neuropilin-2의 중요한 기능적 역할

2022 년 8 월

서울대학교 대학원

치의과학과 분자유전학 전공

안 민 혜

Pivotal functional roles of Neuropilin-2 in cell motility and invasion in head and neck squamous cell carcinoma

두경부 편평상피세포암에서 세포 이동성과
침습능에 대한 Neuropilin-2의 중요한 기능적 역할

지도 교수 백 정 화 / 조 성 대

이 논문을 이학박사 학위논문으로 제출함
2022 년 6 월

서울대학교 대학원
치의과학과 분자유전학 전공
안 민 혜

안민혜의 이학박사 학위논문을 인준함
2022 년 7 월

위 원 장 강 찬 희 (인)

부위원장 백 정 화 (인)

위 원 이 성 중 (인)

위 원 강 세 찬 (인)

위 원 조 성 대 (인)

Abstract

Pivotal functional roles of Neuropilin-2 in cell motility and invasion in head and neck squamous cell carcinoma

Min-Hye Ahn
Program in Molecular Genetics
Department of Dental Science, Graduate School
Seoul National University
Supervised by Professor Jeong-Hwa Baek, D.D.S., Ph.D.
Supervised by Professor Sung-Dae Cho, D.V.M., Ph.D.

Objective

Metastasis is a hallmark of cancer, a process that spreads to nearby or distant locations, and other secondary sites, and it is a major cause of cancer mortality. One of the metastatic cascades that characterize cell motility and invasiveness alters cell-to-cell and cell-to-matrix adhesion and transforms cellular morphology through epithelial-mesenchymal transition (EMT). Neuropilin-2 (NRP2) is mainly known as a single-transmembrane receptor involved in lymphangiogenesis, neuronal development, and angiogenesis by

binding ligands such as vascular endothelial growth factors (VEGFs) or semaphorins (SEMAs) in human diseases, but the molecular mechanism of cell motility and invasiveness in head and neck cancer (HNC) remains unknown. Here, the objective of this study would be to investigate the pivotal functional roles of NRP2 in HNC and its clinical association with lymph node metastasis (LNM) in oral squamous cell carcinoma (OSCC) patients.

Methods

To check the expression pattern of NRP2 in HNC, I utilized University of Alabama Cancer (UALCAN), cBio Cancer Genomics Portal (cBioportal), Cell Line Encyclopedia (CCLE), Gene Expression Omnibus (GEO), The Cancer Genome Atlas (TCGA), and Clinical Proteomic Tumor Analysis Consortium (CPTAC) databases *in silico* analysis and performed immunohistochemistry (IHC) staining to confirm clinical-pathological association with NRP2 and OSCC tissues. Next, to investigate pivotal functions of NRP2 signaling, I also executed MTS assay, soft agar assay, clonogenic assay, immunoblotting, collagen-coated transwell migration, boyden

chamber matrigel-coated invasion assay, and sphere formation assay in NRP2 knockdown or overexpression (O/E) stable HNC cell lines. I screened 20 marine algae extracts to find NRP2-targeting candidate materials using MTS assay and immunoblotting and performed to check the effects of the methanol extracts of *Codium fragile* (MECF) on immunoblotting, collagen-coated transwell migration, boyden chamber matrigel-coated invasion assay, and sphere formation assay in HNC cell lines.

Results

I found that the mRNA expression level of NRP2 was positively correlated with gene copy number in HNC, and NRP2 expression was higher in HNC patient tissues compared with normal tissues *in silico* analysis. The intensity of NRP2 expression in OSCC patient tissues was aberrantly higher than in the adjacent normal epithelium and high expression of NRP2 was significantly associated with LNM and poor prognosis. I demonstrated that NRP2 knockdown suppressed proliferation, colony formation, migratory or invasive ability, and tumor sphere formation in the HNC cell lines, whereas NRP2 O/E

increased these functions. Mechanistically, I demonstrated that p90 ribosomal S6 kinase 1 (RSK1) was a downstream kinase of NRP2 and that the downregulation of RSK1 and phospho-p90 S6 kinase (p-p90RSK$^{T359/S363}$) effectively reduced Sox2, which contributes to cancer stem cell (CSC) properties. I also found that the key EMT marker regulated by NRP2/RSK1/Sox2 axis was Zeb1. Among 20 marine algae extracts, I found that MECF reduced the expression level of NRP2 without changing cell viability and MECF targeting NRP2 exerted anti-metastatic activity through the NRP2/RSK1/Sox2 axis in HNC cell lines.

Conclusion

This study suggests that the NRP2/RSK1/Sox2 axis exerts cell motility and invasiveness by influencing the EMT process and that MECF targeting NRP2 contributes to its anti-metastatic effect in human HNC cell lines.

Keywords : Head and neck cancer, Neuropilin-2, Metastasis, Epithelial-mesenchymal transition, *Codium fragile*

Student Number : 2017-23884

Table of Contents

List of Tables

List of Figures

Ⅰ. Introduction

Head and neck cancer (HNC) encompassing the lip, oral cavity, larynx, nasopharynx, oropharynx, hypopharynx, and salivary glands is the seventh most common cancer worldwide as of GLOBOCAN in 2020 (Sung et al, 2021). It was estimated that newly diagnosed cancer cases every year were taken up by 93 thousand cases (4.9 %) out of 19.3 million cases, and cancer mortality was occupied by 46 thousand cases (4.7 %) out of 10 million cases. The impact of most histological malignancies occurs in squamous cell carcinoma (SCC), usually of epithelial origin, accounting for more than 90 % of HNCs. The incidence of traditional risk factors was caused by cigarette smoking and alcohol consumption, and human papillomavirus infection has also been recognized to promote carcinogenesis. Other risk factors were identified, such as heredity, dietary life, toxic exposure, and environmental factors (Cohen et al, 2018). The treatment options of HNC patients depend on the stage of the disease, anatomical site, and surgical accessibility, and currently radiation therapy and chemotherapy are combined with surgical resection (Marur and

Forastiere, 2008). Despite this comprehensive and advanced therapy, more than 65 % of HNC patients have relapsed or metastasized to distant locations (Chow, 2020). About 40 % of the lymph nodes of the human body are located within the head and neck and are well-known as one of the important predictors of poor prognosis for HNC patients (Harisinghani and SpringerLink, 2013, Karatzanis et al, 2012). In the early events of the metastatic process, tumor cells are disseminated to regional lymph nodes, and newly formed lymphatic vessels serve as the primary routes for its purpose (Wissmann and Detmar, 2006). Several reports have shown that growth factors are involved to promote the spread of malignant diseases by leading to the development of lymphatic vessels within intra- and peri-tumoral environments (Zhang et al, 2010). VEGF-C and VEGF-F bind to the VEGF receptor-3 (VEGFR-3) to exert lymphangiogenic activity, which causes the growth and migration of the lymphatic endothelial cells in some cancer types such as HNC, lung, colorectal, and breast cancer (Karatzanis et al, 2012, Kajita et al, 2001, Akagi et al, 2000, Salven et al, 1998). In particular, increased expression of VEGF-C and VEGF-D in OSCC has been reported to be significantly

associated with lymph node metastasis and poor prognosis (Shintani et al, 2004).

Neuropilins (NRP1 and NRP2) were first identified in vertebrates as single-transmembrane glycoproteins that are co-receptors for specific members of the VEGF family of angiogenic cytokines (Staton et al, 2007). NRP1 and NRP2 have a similar domain structure with 44 % of an amino acid homology (Chen et al, 1997) and were for the first time found to play roles in regulating axon guidance (Pellet-Many et al, 2008). NRP1 is mainly necessary for normal embryonic development of the nervous and cardiovascular systems (Kawasaki et al, 1999), and NRP2 acts primarily on the regulation of lymphangiogenesis (Yuan et al, 2002). Both NRPs interact with SEMAs or VEGFs, which promote tumor growth, migration, and invasion in some epithelial cells derived from several organs (Pellet-Many et al, 2008). NRP2 is highly expressed in a variety of malignant tumor cells or tissues (Bielenberg et al, 2006) and promotes neovascularization, which causes tumor progression and metastasis in numerous cancer types, including breast cancer (Yasuoka et al, 2009), non-small cell lung cancer (Kawakami et al, 2002), colorectal

cancer (Gray et al, 2008), and recurrent lymphangioma (Yan et al, 2020). It has recently been demonstrated that overexpression of NRP2 in colorectal carcinoma (Grandclement et al, 2011) and hepatocellular carcinoma (Wittmann et al, 2015) induces transforming growth factor $\beta 1$ (TGF$-\beta 1$) signaling, leading to tumor progression and metastasis by regulating EMT (Prud'homme and Glinka, 2012). However, most of the current studies are based upon lymphangiogenesis and angiogenesis, and the pivotal functional role of NRP2 underlying the metastatic behaviors of HNC remains to be fully elucidated.

More than 80 % of innumerable organisms including animal, plant, bacteria, fungi, and protist in the five kingdoms of Earth, have inhabited and thrived in the oceans for 2 to 3 billion years (Donia and Hamann, 2003). Depending on oxygenic photosynthesis, fluctuations in the habitat salinity, water temperature, and geographical conditions, the marine environment factors accompanied the biological megadiversity (Rioux et al, 2009), and then a variety of novel active natural compounds have been discovered with an increasing trend from 1985 to 2012 (Hu et al, 2015, Bhardwaj et al, 2021). These

marine-originated compounds have been recognized as prospective resources for the development of the nutraceuticals and pharmaceuticals field (Thomas and Kim, 2013). Sulfated polysaccharides in which some of the hydroxyl groups of sugar residues are substituted with sulfate groups were acquired from red algae (Rhodophyta), brown algae (Ochrophyta-Phaeophyceae), and green algae (Chlorophyta). These sulfated polysaccharides are well known to exhibit various biological activities (Lee et al, 2010) such as anticancer (Lin et al, 2020), anticoagulant (Pomin, 2012), and antiviral effects (Lee et al, 2004). *Codium fragile*, belonging to the genus of approximately 150 species of *Codium*, is a dark green alga. These algae have finger-shaped cylindrical nodes with a soft surface that branch repeatedly and are widely distributed in East Asia, Oceania, and Northern Europe along the seaside (Tabarsa et al, 2013, Verbruggen et al, 2007). To date, there are several studies regarding the efficacy of *C. fragile* extracts or isolated single compounds (Dilshara et al, 2016, Ganesan et al, 2010, Choi et al, 2013, Ohta et al, 2009). Dilshara et al. reported that the MECF suppressed invasiveness of MDA-MB-231 cells by inhibiting tumor necrosis

factor-α-induced matrix metalloproteinase-9 and nuclear factor-κB activation (Dilshara et al, 2016). Siphonaxanthin, which is a specific keto-carotenoid isolated from *C. fragile*, reduced tube formation in HUVEC cells and inhibited microvessel outgrowth *ex vivo* (Ganesan et al, 2010). An enzyme with fibrinolytic serine protease function purified from *C. fragile* has anticoagulant and antiplatelet activities (Choi et al, 2013). From spectroscopic analyses, sulfated galactan isolated from *C. fragile* suppressed herpes simplex virus type 2 activity *in vitro* and *in vivo* (Ohta et al, 2009). However, the crucial roles of MECF based on cell migration and invasiveness are still unknown.

The aim of my study is to identify that the expression level of NRP2 has clinical relevance in OSCC patients and to elucidate the pivotal functional roles of NRP2 on cell motility and invasiveness in HNC cell lines and underlying molecular mechanism. In addition, I also attempted to discover a marine-originated compound targeting NRP2 as a potential chemotherapeutic candidate for the treatment of metastatic HNC.

Ⅱ. Materials and Methods

in silico analysis

UALCAN

The UALCAN database (http://ualcan.path.uab.edu/) is a web resource for analyzing cancer OMICS data including TCGA. It was utilized to analyze the NRP2 expression in normal tissues and multiple primary tumor tissues (Chandrashekar et al, 2017). All five values of each box plot were recorded and replotted using GraphPad Prism version 8.4 software (GraphPad Software, San Diego, CA, USA).

cBioportal

An open-access resource, cBioportal (http://cbioportal.org) is a multidimensional cancer genomics database (Cerami et al, 2012). The correlation between genetic putative copy-number and mRNA expression level (RNA Seq V2 RSEM with z-scores = ±2) of NRP2 was assessed for the HNC using the TCGA PanCan 2018 dataset.

CCLE

Following public access to genomic data from CCLE (https://depmap.org/por-tal/ccle/), correlations between the copy number and mRNA expression level of NRP2 were estimated according to specific genetic characteristics of upper aerodigestive cancer cell lines including tongue SCC; oral cavity SCC; gingival SCC; and SCC of the lower alveolus in the customized cohorts.

GEO database

The GEO (https://www.ncbi.nlm.nih.gov/geo/) is a public genomics database and can be used to explore the mRNA expression level of NRP2 for HNC (Barrett et al, 2013). Variation in NRP1 (8829_at) and NRP2 (8828_at) mRNA levels between the normal (n=24), margin (n=45), and cancer (n=23) groups was analyzed using geo series GSE31056. Variation in NRP1 mRNA levels between the normal (n=45), dysplasia (n=17), and cancer (n=167) groups was evaluated using geo series GSE30784 reporter identifier 210615_at, 212298_at, and 1561365_at. Variation in NRP2 mRNA levels between the normal (n=45), dysplasia (n=17), and cancer (n=167) groups

was evaluated using geo series GSE30784 reporter identifier 222877_at and 229225_at. The Pearson's correlations between NRP2 (222877_at) and VEGFR-1/2/3 mRNA levels were analyzed using geo series GSE30784. Variation in NRP2 mRNA levels was analyzed within the same cases between adjacent non-tumor epithelium (n=40) and cancer (n=40) using geo series GSE37991 reporter identifier ILMN_2376484. Variations in NRP2 mRNA levels were also investigated between negative (n=40) and positive (n=54) LNM using geo series GSE30788 reporter identifier Agendia_DiscoverPrint_HN_probe_44745. All extracted data were normalized using Geo2R.

TCGA database

Following the assessment of the HNC dataset via TCGA database (https://portal.gdc.cancer.gov/), a custom cohort was categorized including base of tongue, lip, palate, gum, tonsil, floor of mouth; other and unspecified parts of mouth; other and unspecified parts of tongue; and other and ill-defined sites in lip, oral cavity and pharynx. The series of data trimming were analyzed using Jupyter notebook and

Pandas on top of Pyton 3.0 and the code can be used at https://github.com/kunalchawlaa/TCGA-Oral-Cancer. The mRNA expression level of NRP2 was evaluated to compare normal (n=32) and HNC (n=369) using FPKM-UQ files.

CPTAC

CPTAC database (https://pdc.cancer.gov/pdc/) can retrieve proteo-genomic analysis of diverse cancer types (Huang et al, 2021). Proteomic data of NRP2 were obtained from the HNC Discovery Study database including the base of tongue not otherwise specified (NOS), tongue NOS, lip NOS, gum NOS, tonsil NOS, floor of mouth NOS, cheek mucosa, head of face or neck NOS; and overlapping lesion of lip, oral cavity and pharynx. Reporter ion intensity log2 ratio unshared peptides of NRP1 and NRP2 values were shown to compare the expression level of normal (n=31) and cancer (n=57). NRP2 was analyzed for Pearson's correlation with NRP1, Sox2, or VEGFR-1 protein levels.

Analysis of Relative risk (RR) and Confidence intervals (CIs)

The RR and 95 % CIs were estimated between the low NRP2 expression group and the high NRP2 expression group based on clinicopathological factors such as age, sex, tumor size, LNM, primary tumor stage, and recurrence in OSCC patients. The values were calculated using MedCalc® statistical software (https://www.-medcalc.org/calc/relative_risk.php) and were expressed as a forest plot using GraphPad Prism version 8.04.

Kaplan-Meier (KM) Plotter survival analysis

KM plotter (http://kmplot.com/analysis), an online survival software (Nagy et al, 2021), can analyze the overall survival (OS) rate of cohorts with differential NRP2 expression levels in HNC patients.

Clinical tissue samples

In this retrospective study, a total of 53 tissues with OSCC were retrieved from patients who underwent surgical treatment for IHC staining at the Department of Oral Maxillofacial Surgery at Seoul National University Dental Hospital (Seoul, Republic of Korea)

between 2006 and 2007. Classification of malignancy for TNM system was provided by the American Joint Committee on Cancer manual (Amin et al, 2017). Tumor grades were based on the World Health Organization (El-Naggar, 2017). The clinicopathological factors including age, gender, TNM classification, tumor stage, and recurrence were collected from medical records. The characteristics of 53 patients are specified in Table 4. The present study was approved by the Institutional Review Board (IRB) of Seoul National University Dental Hospital (IRB No. ERI20021).

IHC staining

Paraffin-embedded tissues from OSCC patients were sectioned at a thickness of 3.5 μm, and after holding at 60 ℃ for 30 min to melt paraffin. Sequentially, Specimens were washed with neo-clear to remove paraffin and graded ethanol to proceed with the rehydration process. For antigen retrieval, after heating to high temperature in antigen retrieval citrate buffer (pH 6.0) using a microwave oven for 10 min, Peroxidase Blocking Reagent (Dako, Carprinteria, CA, USA) was reacted to inactivate endogenous peroxidase activity for 5 min.

Sections were incubated with a mouse polyclonal anti NRP2 antibody (1:100, Santa Cruz, CA, USA) overnight at 4 ℃ in a humidified chamber. Next day, the sections were reacted using REAL™ EnVision™/ horseradish peroxidase (HRP) Rabbit/Mouse (Dako) in a humidified chamber at room temperature for 30 min and were carried out by mixing REAL™ DAB and Chromogen with Substrate Buffer (Dako) for a color reaction for 5 min. the sections were counterstained with hematoxylin, dehydrated, and mounted using Permount solution (Thermo Fisher Scientific, Waltham, MA, USA).

Assessment of IHC staining

IHC staining sections were semi-quantitatively evaluated and independently reviewed by two oral pathologists without clinicopathological knowledge of the patients' outcomes. If there was a slight disagreement between two observers, they got reappraisal to a consensus review. The definition of tumor proportion score (TPS) was classified as follow: 0, 0 %; 1, 1-4 %; 2, 5-49 %; and 3, 50-100 %. Staining intensity was scored as follows: 0, negative; 1, weak (light brown); and 2, strong (brown). The final score was the TPS

multiplied by the value of intensity and was derived from 0 to 9. For statistical assessment, the final score was categorized according to low expression (≤4) or high expression (>4).

Cell culture

The human oral keratinocyte (HOK) cell line was purchased from Lifeline cell technology (Oceanside, CA, USA). The Ca9.22 (CVCL_1102, derived from a patient with gingiva SCC of the oral cavity), HSC-2 (CVCL_1287, derived from a metastatic cervical lymph node in a patient with SCC of the floor of mouth), HSC-3 (CVCL_1288, derived from a metastatic cervical lymph node in patient with tongue SCC), and HSC-4 (CVCL_1289, derived from a metastatic cervical lymph node in a patient with tongue SCC) cell lines were kindly provided by Hokkaido University (Hokkaido, Japan). The FaDu (CVCL_1218, derived from a patient with hypopharyngeal SCC), YD-15 (CVCL_8930, derived from a patient with mucoepidermoid carcinoma of the oral tongue), and YD-15M (CVCL_L078, derived from a metastatic lymph node in patient with mucoepidermoid carcinoma of the oral tongue) cell lines were

purchased from the Korean Cell Line Bank (Seoul, Republic of Korea). The HN22 cell line (CVCL_5522, derived from a patient with SCC of the epiglottis) was obtained from Dankook University (Cheonan, Republic of Korea). The MC-3 (derived from a patient with mucoepidermoid carcinoma) cell line was provided by Fourth Military Medical University (Xi'an, China). The HOK cell line was maintained in DermaLife K keratinocyte Medium Complete Kit (Lifeline cell technology). The Ca9.22, HSC-2, HSC-3, HSC-4, HN22, and MC-3 were cultured in Dulbecco's modified essential medium/F-12 Nutrient Mixture Ham (WELGENE, Gyeongsan, Republic of Korea). The YD-15 and YD-15M cell lines were grown in Roswell Park Memorial Institute 1640 medium (WELGENE). The FaDu cell line was cultured in a modified essential medium (MEM). All media for HNC cell lines were supplemented with 10 % fetal bovine serum (FBS) and 1 % penicillin/streptomycin (P/S) in a humidified atmosphere containing 5 % CO_2 at 37 ℃. Cells were washed with Dulbecco's phosphate-buffered saline (DPBS) (WELGENE). All experiments were carried out when almost 50 % cell confluency was reached.

Preparation of algae extracts and chemicals

The methanol extracts of algae samples were kindly provided by the Marine Brown Algae Resources Bank (Unique identifier: TC9305) of Chosun University (Gwangju, Republic of Korea). The methanol extracts of algae are listed in Table 1. RSK inhibitor, BI-D1870 was synthesized by abcam (Cambridge, MA, USA). The extracts of algae and BI-D1870 were dissolved in dimethyl sulfoxide (DMSO), aliquoted, and stored at −20 ℃ until used. The final concentration of DMSO for each cell line did not exceed 0.1 %. Human basic fibroblast growth factor (bFGF) Recombinant Protein, Human epidermal growth factor (EGF) Recombinant Protein, N-2 Supplement (100X), and B-27 Supplement (50X) were purchased from Gibco (Life Technologies, Darmstadt, Germany). Basal Medium Eagle (BME) and Sodium bicarbonate were purchased from Sigma Aldrich (St. Louis, USA). L-glutamine was purchased from Corning (NY, USA) and Gentamicin sulfate was purchased from Lonza (Basel, Switzerland).

Plasmid construction

To stably and specifically knockdown NRP2 in the HSC-4, FaDu, and HN22 cell lines, the synthesized DNA oligos containing short hairpin RNA (shRNA) sequences were cloned into lentiviral pLKO.1 vector (Addgene, Cambridge, MA, USA). Scramble RNA (scramble) was used as a control vector (Addgene). The forward sequence for shNRP2 was (F) 5'-CCG GGC CAT TGA TGA CAT TCG GAT ACT CGA GTA TCC GAA TGT CAT CAA TGG CTT TTT G-3' and the reverse sequence for shNRP2 was (R) 5'-AAT TCA AAA AGC CAT TGA TGA CAT TCG GAT ACT CGA GTA TCC GAA TGT CAT CAA TGG C -3'. To overexpress NRP2 in the HSC-2 cell line, the open reading frame of NRP2 was synthesized from Bioneer (Daejeon, Republic of Korea) and cloned into the multi-cloning site of a pBabe puro IRES-EGFP vector (Addgene).

Stable transfection and virus infection

For lentiviral packaging using knockdown of NRP2 system, HEK 293T cells were grown to almost 100 % confluency and were transfected with scramble or shNRP2 together with pCMV-dR8.2

dvpr packaging vector and pCMV-VSV-G envelope vector (Addgene). For retroviral packaging using overexpression of NRP2 system, HEK 293T cells were transfected with empty pBabe puro IRES-EGFP or pBabe-NRP2 expression vector along with pCL-10A1 packaging plasmid (Novus Biologicals, Littleton, CO, USA). All transfection procedures were carried out using Lipofectamine 2000 (Promega, Madison, USA) following the manufacturer's instructions. After 48 h post-transfection, the viral supernatants were collected and filtered through a 0.45 μm syringe filter to remove debris. Purified viral supernatants were added to the target cells with 6 μg/ml of polybrene and transduced for 30 to 48 h. In order to select transfected cells, 0.5 μg/ml of puromycin was treated.

Immunoblotting

Total Protein lysates of cells and tissues were obtained for 15 min at 4 ℃ in 1X RIPA buffer (EMD Millipore, Billerica, MA, USA) containing cOmplete™ Mini EDTA-free Protease Inhibitor Cocktail (Merck, Darmstadt, Germany) and Pierce™ phosphatase inhibitor tablets (Thermo Fisher Scientific). The determination of protein

concentration was used by DC Protein Assay Kit (BIO-RAD Laboratories, Madison, WI, USA), and then the equivalent of total protein was boiled with 5X protein sample buffer (ELPIS Biotech, Daejeon, Republic of Korea) for 5 min at 95 ℃. Proteins were separated by sodium dodecyl sulfate polyacrylamide gel electrophoresis and then transferred to 0.2 μm Immuno-Blot polyvinylidene fluoride membranes (Thermo Fisher Scientific). After blocking with 5 % skim milk dissolved tris-buffered saline with Tween 20 (TBST) by rocking for 2 h, the membranes were then reacted with primary antibodies overnight at 4 ℃. After washing with TBST, the membranes were incubated with HRP-conjugated secondary antibodies (GeneTex Inc., Irvine, CA, USA) for 2 h at 4 ℃. Blots were visualized using WestGlowTM FEMTO Chemiluminescent Substrate (BIOMAX, Seoul, Republic of Korea) followed by X-ray film or ImageQuant LAS500 (GE Healthcare Life Sciences, Piscataway, NJ, USA). The protein expression levels were measured by ImageJ software (National Institutes of Health, Bethesda, USA) and normalized to the level of β-actin. Primary antibody information is shown in Table 2.

Quantitative RT-PCR

Total RNA was extracted using TRIzol reagent (Life Technologies, Carlsbad, CA, USA) according to the manufacturer's instructions. Reverse transcription for cDNA was synthesized with AMPIGENE cDNA Synthesis kit (Enzo Life Sciences, Inc., NY, USA). qPCR was carried out with AMPIGENE qPCR Green Mix Hit-Rox (Enzo Life Sciences) on the Applied Biosystems StepOne Plus Real-Time PCR system (Applied Biosystems, CA, USA). the qPCR conditions were as follows: Initial activation at 95 ℃ for 2 min, followed by 40 cycles of denaturation at 95 ℃ for 10 sec, annealing at 60 ℃ for 30 sec, and extension at 60 ℃ for 1 min. Cycle threshold (CT) values were determined and the relative expression of RNA expression was calculated by using the values of $2^{-\triangle\triangle CT}$. Each RNA expression level was normalized to the *GAPDH* gene. The primer sequences used in this study are listed in Table 3.

[3-(4,5-dimethylthiazol-2-yl)-5-(3-carboxymethoxyphenyl)-2-(4-sulfophenyl)-2H-tetrazolium] (MTS) assay

MTS assay was performed to confirm the comparison of cell

proliferation on the NRP2 knockdown three stable HSC-4, FaDu, and HN22 cell lines compared to scramble cells. It was also used to measure the cytotoxicity of 20 methanol extracts of algae in HSC-4 cell line. According to the manufacturer's instructions, the MTS mixture solution was made up of the CellTiter 96® AQueous One Solution Reagent and electron coupling reagent phenazine methosulfate (Promega). Cells were seeded in 96 well plates and incubated at 37 ℃. Briefly, 40 μl of MTS mixture solution was added to each well and incubated for 2 h at 37 ℃ while blocking out light. After incubation, the absorbance of each well was measured at 482 nm using a microplate reader (Hidex, Turku, Finland).

Soft agar assay

Soft agar assays were performed to assess anchorage-independent growth ability by culturing stable knockdown or overexpression cell lines (Borowicz et al, 2014). Briefly, BME and sodium carbonate were dissolved in sterile distilled water to make 2X BME and then purified with a 0.2 μm syringe filter. The 0.5 % bottom agar was prepared by mixing 2X BME, L-glutamine, gentamicin, PBS, FBS, and

1.25 % agar and then was pre-coated with 3 ml per well of 6-well plates. Cells were trypsinized and seeded at 0.8 × 10^4 cells per well with 0.3 % top agar. After curing again at room temperature for 1 h, 200 μl of culture medium was added weekly to prevent desiccation and incubation at 37 ℃ for 10 to 14 days. Images of the colonies were randomly selected for 4 photos per well and taken a photograph under a microscope (Olympus, Tokyo, Japan) at a 40 X magnification and the number of colonies was calculated manually using ImageJ software.

Clonogenic forming assay

NRP2 knockdown or overexpression stable cell lines were seeded at 2.5 × 10^3 cells per well into 6-well plates, and the culture media were replaced after 3 days. On day 7, cells were fixed with 100 % methanol for 10 min, stained with 1 % crystal violet in 20 % methanol for 30 min, and washed 3 times with distilled water. The number of stained colonies was taken a picture through a light microscope.

Transwell migration assay

Transwell migration assays were performed to assess the ability of migration on HNC cell lines. Briefly, 24-well Falcon® Cell Culture Inserts (Corning) with PET membranes of 8.0-μm pore size were coated with Collagen I (BD Bioscience, Bedford, MA, USA) at a concentration of 0.5 mg/ml for 4 h at room temperature. Cells in serum-free medium were seeded in the upper chamber and 500 μl of medium containing 10 % FBS was added to the lower chamber. After incubation for 24 h or 48 h at 37 ℃, the non-migratory cells from the top of the membrane were wiped off with a cotton swab. The cells on the lower chamber side were fixed with 100 % methanol for 2 min and stained with hematoxylin for 10 min, followed by eosin for 2 min. The stained cells were photographed using an inverted light microscope (Nikon, Tokyo, Japan) and counted in four randomly selected areas of the membrane.

Boyden chamber transwell invasion assay

Boyden chamber transwell invasion assays were carried out to test the capacity of invasiveness on HNC cell lines. Briefly, the Corning®

Matrigel® Growth Factor Reduced Basement Membrane Matrix (Corning) was mixed with serum-free medium in the ratio of 1:15. The same 24-well Falcon® Cell Culture Inserts were coated with 100 ㎕ mixture inner side of the upper chamber and incubated at 37 ℃ for 2 h. Prior to seeding, the mixture was aspirated from the upper chamber and washed twice with 100 ㎕ serum-free medium. Cells in serum-free medium were seeded in the upper chamber and 500 ㎕ of medium containing 10 % FBS was added to the lower chamber. After incubation for 24 h or 48 h at 37 ℃, the non-invaded cells from the top of the membrane were wiped off with a cotton swab, and the cells on the lower chamber side were fixed with 100 % methanol for 2 min and stained with 1 % crystal violet diluted in 20 % methanol for 30 min. The stained cells were photographed using an inverted light microscope (Nikon) and counted in four randomly chosen areas of the membrane.

Small-interfering RNA (siRNA) transfection

According to the manufacturer's instructions, Lipofectamine 2000 (Promega), AccuTarget™ Negative Control siRNA (sicontrol) or

Sox2 siRNA (siSox2), were diluted with Opti-MEM (Gibco) and then stabilized for 5 min. Next, each solution was mixed gently and incubated for 20 min at room temperature. Cells were treated to transfect when the confluency reached about 40-50 %. After incubation (24 h for FaDu and 48 h for HSC-4), the interference efficiency was confirmed by Immunoblotting. sicontrol and siSox2 were purchased from Bioneer and target sequences were described as follows: Human Sox2; Sense 5'-GCA GCU GAA AUU UAG GAC A-3', Human Sox2; Anti sense 5'-UGU CCU AAA UUU CAG CUG C-3'

Sphere formation assay

Cells were cultured in a serum-free medium containing 25 ng/ml of EGF and bFGF, 0.01X of N-2, B-27 supplement, and 1 % P/S and were seeded into ultra-low attachment 6-well plates (Corning) at a density of $5 \times 10^3 - 1 \times 10^4$ of cells per well. 7-10 days after seeding, the number of spheres larger than 50 μm in diameter was randomly captured and counted using an inverted light microscope (Nikon) and ImageJ software, respectively.

Proteomic profiling

The 1,358 differentially expressed proteins were analyzed in the NRP2 knockdown stable HSC-4 cell line. Significantly expressed proteins by more than 1.2-fold change were selected and identified. Data mining and graphical visualization were carried out using Excel Based Differentially Expressed Gene Analysis (ExDEGA) v2.5.0 software (EBIOGEN, Seoul, Korea).

Trypan blue exclusion assay

The cells were detached from the plate with a 0.25 % trypsin-EDTA solution (WELGENE) and suspended in 1 ml of PBS. Cells were stained with 0.4 % trypan blue solution (Gibco), and the fraction of viable cells was counted using a hemocytometer.

Statistical analysis

In accordance with *in silico* studies, comparisons between normal and tumor tissues; or non-metastasis and metastasis were used with an unpaired or paired two-tailed Student's t-test. Spearman's correlation coefficient was conducted to compare between DNA copy

number and mRNA expression levels. For *in vitro* data, a two-tailed Student's t-test was performed difference between the experimental groups. Immunohistochemical data and clinicopathological features were followed by a multivariable Pearson chi-square test. All data analyses were expressed using GraphPad Prism version 8.4 and were evaluated using SPSS 25 (SPSS, Chicago, IL, USA). In general, experiments were conducted independently in triplicate. $P < 0.05$ was considered statistically significant.

Table 1. Cytotoxicity of algae on HSC-4 cell line.

	Name	Family	Viability (%)
1	*Sargassum horneri*	Sargassaceae	97.96
2	*Colpomenia sinuosa*	Scytosiphonaceae	98.04
3	*Agarum clathratum*	Agaraceae	94.4
4	*Sargassum pallidum*	Sargassaceae	96.04
5	*Sargassum muticum*	Sargassaceae	95.94
6	*Sargassum sagamianum*	Sargassaceae	94.96
7	*Dictyopteris pacifica*	Dictyotaceae	92.89
8	*Mutimo cylindricus*	Cutleriaceae	93.82
9	*Sargassum micracanthum*	Sargassaceae	105.32
10	*Undaria pinnatifida*	Alariaceae	98.86
11	*Padina arborescens*	Dictyotaceae	96.95
12	*Dictyopteris divaricata*	Dictyotaceae	101.68
13	*Ecklonia cava*	Lessoniaceae	101.89
14	*Polyopes sp.2*	Halymeniaceae	99.49
15	*Ulva australis*	Ulvaceae	94.71
16	*Saccharina japonica*	Laminariaceae	92.7
17	*Codium fragile*	Codiaceae	97.67
18	*Sargassum fusiforme*	Sargassaceae	100.96
19	*Capsosiphon fulvescens*	Ulotrichaceae	101.07
20	*Gloiopeltis tenax*	Endocladiaceae	102.12

Table 2. Antibody information used in Immunoblotting.

Protein (size)	Source	Company (Catalogue)	Dilution
NRP2 (116 kDa)	Mouse	Santa Cruz Biotechnology (SC-13117)	1:1000
p-p90RSK $^{(T359/S363)}$ (90 kDa)	Rabbit	Cell Signaling Technology (#9344)	1:1000
RSK1 (90 kDa)	Rabbit	Cell Signaling Technology (#9333)	1:1000
Sox2 (37 kDa)	Rabbit	Abcam (ab97959)	1:1000
Sox2 (37 kDa)	Rabbit	Cell Signaling Technology (#14962)	1:1000
Nanog (40 kDa)	Rabbit	Abcam (ab80892)	1:1000
Oct4 (50 kDa)	Rabbit	Abcam (ab19857)	1:1000
Zeb1 (130 kDa)	Rabbit	Novus Biologicals (NBP1-05987)	1:1000
Zeb2 (128 kDa)	Mouse	Santa Cruz Biotechnology (SC-271984)	1:1000
E-Cadherin (120 kDa)	Mouse	BD Transduction Laboratories (#610181)	1:1500
ZO-1 (220 kDa)	Rabbit	Cell Signaling Technology (#8193)	1:1000
Twist (28 kDa)	Mouse	Santa Cruz Biotechnology (SC-81417)	1:1000
Slug (30 kDa)	Rabbit	Cell Signaling Technology (#9585)	1:1000
Fibronectin (220 kDa)	Rabbit	Santa Cruz Biotechnology (sc-9068)	1:1000
β-actin (43 kDa)	Mouse	Santa Cruz Biotechnology (SC-47778)	1:3000

Table 3. Primer sequences used in quantitative RT-PCR

Target gene	Direction	Sequence	Product size
NRP2	F	5' -CCAAGAGCCACTAGAGAACTTT-3'	106 bp
	R	5' -CCTCCCATCAGAGTAGGTAGAT-3'	
GAPDH	F	5' -GTGGTCTCCTCTGACTTCAAC-3'	129 bp
	R	5' -CCTGTTGCTGTAGCCAAATTC-3'	

Table 4. Clinicopathological features of 53 OSCC patients

Variable	No. of cases (%)
Age (years; mean, 57.8)	
20–29	2 (4)
30–39	4 (8)
40–49	10 (19)
50–59	12 (23)
60–69	12 (23)
70–79	10 (19)
≥80–89	3 (6)
Gender	
Male	36 (68)
Female	17 (32)
Differentiation status	
Well	36 (68)
Moderately	17 (32)
T classification	
T1	15 (28)
T2	17 (32)
T3	3 (6)
T4	18 (34)
N classification	
N0	32 (60)
N1	7 (13)
N2	14 (26)
M classification	
M0	52 (98)
M1	1 (2)
Stage	
I	12 (23)
II	12 (23)
III	7 (13)
Ⅳ	22 (42)
Recurrence	
No	41 (77)
Yes	12 (23)

Ⅲ. Results

1. Aberrant expression of NRP2 is positively associated with LNM in human HNC.

To investigate the clinical relevance of NRP2 in human pathogenesis, I performed *in silico* analysis to evaluate the expression of NRP2 in different cancer types. I used UALCAN to access TCGA pan-cancer dataset to analyze the NRP2 expression between 9 kinds of human cancers and corresponding normal tissues. Compared with normal tissues, the expression level of NRP2 was highly increased in various cancers (e.g., Cholangio-carcinoma, Colon adenocarcinoma, Esophageal carcinoma, Thyroid carcinoma, Head and neck carcinoma, etc.) (Figure 1A). I developed the correlation of the gene copy number with NRP2 mRNA expression in HNC via cBioportal and observed that the gene copy number of NRP2 was correlated with its mRNA expression positively ($r = 0.232$, $p = 0.000$, Figure 1B). Consistent with this result, I also showed a trend of positive correlation for cancer cell lines of an upper aerodigestive tract from

CCLE database (Figure 1C). I further plotted the mRNA expression of NRP2 in HNC compared to normal or margin tissues using the GSE31056 8828_at dataset and found that the mRNA expression levels of NRP2 were significantly elevated in HNC tissues compared to normal or margin tissues (Figure 2A). Similar evaluations for both mRNA or protein expression levels of NRP2 between HNC and normal tissues were obtained from TCGA database and CPTAC (Figure 2B and 2C). I also observed that the mRNA expression levels of NRP2 in HNC were upregulated compared to normal according to the development of the carcinogenesis via GEO data set (GSE30784 222877_at and 229225_at) (Figure 2D and 2E). Consistent with these results, a higher mRNA expression level of NRP2 was significantly observed in 40 paired HNC tissues than in adjacent non-tumor epithelium in GEO data set (GSE37991 ILMN_2376484) (Figure 2F). Additionally, I found that both mRNA (GSE31056 8829_at) and protein expression levels of NRP1 were decreased in HNC compared to normal tissues from GEO and CPTAC databases (Figure 3A and 3B). I obtained that the mRNA expression levels of NRP1 were not significantly changed in HNC compared to normal

according to the development of the carcinogenesis via GEO data set (GSE30784 210615_at, 212298_at, and 1561365_at) (Figure 3C–3E). I also found that the protein expression levels between NRP1 and NRP2 have little correlation in HNC from CPTAC (Figure 3F). These results indicated that NRP2 may specifically function in human HNC as a diagnosable malignant parameter.

To confirm the results from *in silico* analysis, IHC analysis was conducted on 53 paired OSCC patient tissues between 2006 and 2007 at Seoul National University Dental Hospital (IRB No. ERI20021). The results showed that the intensity of NRP2 was highly expressed in OSCC tissues compared to the adjacent non–tumor epithelium (Figure 4A). From the process of carcinogenesis and tumor development perspective, the tumor size and stage were associated with overexpression of NRP2, which are listed in Table 5 ($p = 0.001$ and $p < 0.001$, respectively). To further investigate the correlation between NRP2 and OSCC progression, I performed a multivariable analysis between clinicopathologic variables and expressions of NRP2. I found that high NRP2 expressions significantly correlated with advanced tumor size, LNM, and stage, exhibiting a high RR

(Figure 4B).

Importantly, to investigate the association between LNM and the expression intensity of NRP2 in OSCC tissues, different histopathologic variables were identified and categorized through the expression pattern of NRP2. The high expression intensity of NRP2 was correlated with LNM from cohorts of 53 OSCC patients (Figure 5A), and it could present the expression pattern of NRP2 was statistically significant in LNM cases (N1+N2) followed by IHC score ($p = 0.006$) (Figure 5B). Figure 5C showed that the high mRNA expression levels of NRP2 appeared to correlate with positive LNM with HNC tissues in the GEO dataset (GES30788 Agendia_DiscoverPrint_HN_probe_44745) ($p = 0.004$), similar to IHC data. Notably, a close relationship was examined between NRP2 expression and OS rate of HNC patients using the KM plotter, indicating that the high expression of NRP2 was associated with poor OS rate of HNC patients (Figure 5D). These results suggest that aberrant expression of NRP2 was associated with LNM and poor prognosis in human HNC.

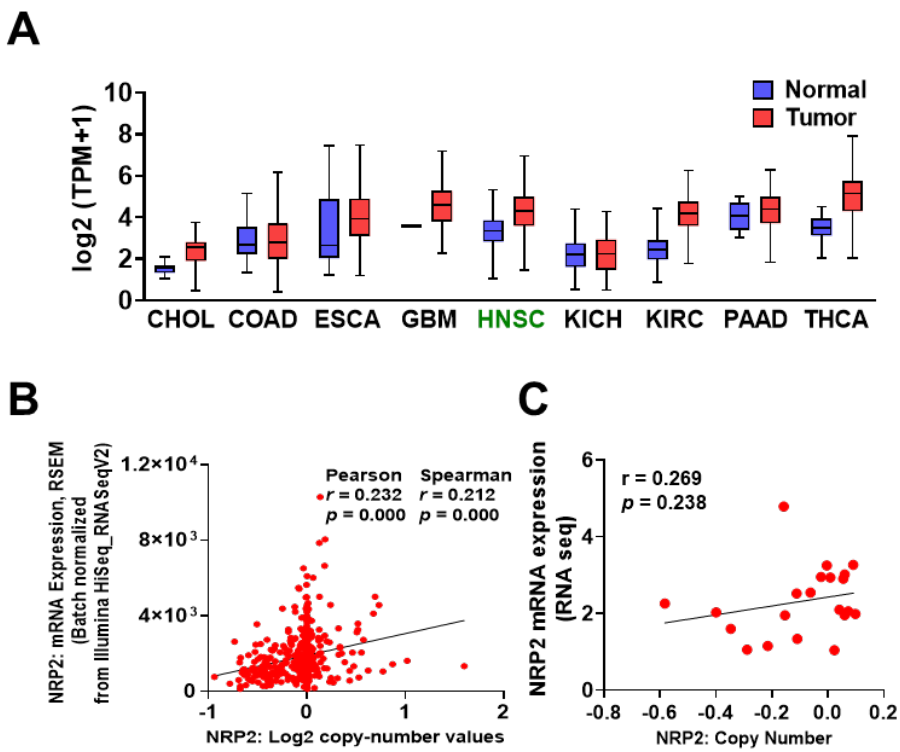

Figure 1. NRP2 is highly expressed in human HNC. (A) The transcripts per million of NRP2 were overexpressed across 9 kinds of human cancer types using ULACAN. (B) A positive correlation between NRP2 gene copy number and mRNA levels was represented in HNC using cBioportal. The correlation coefficients were evaluated by Pearson's and Spearman's correlation tests. (C) A positive correlation between NRP2 gene copy number and mRNA levels was represented in various oral cancer cell lines using CCLE.

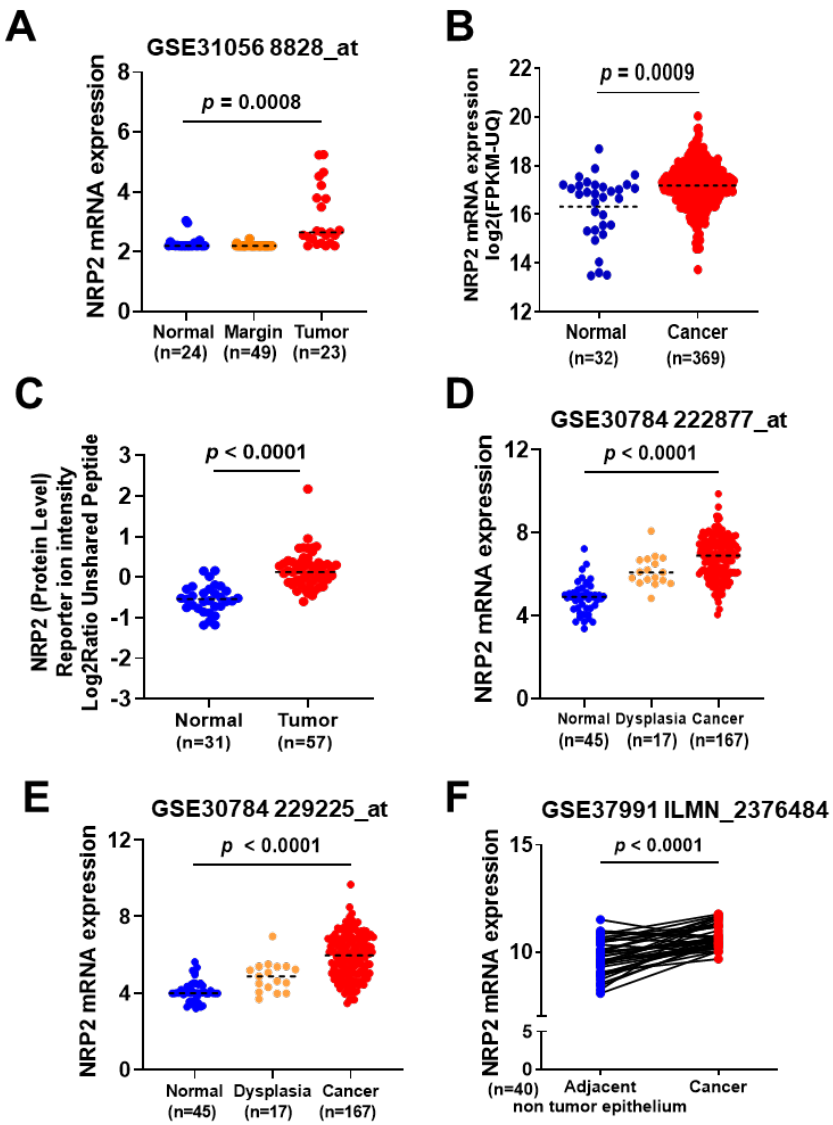

Figure 2. The expression of NRP2 is frequently upregulated in human HNC. (A) The mRNA expression levels of NRP2 were significantly upregulated in HNC in the comparison with normal and margin tissue

from GEO dataset (GSE31056). (B) Upregulation of NRP2 mRNA levels was shown in HNC cancer compared to normal tissue using TCGA dataset. (C) The protein expression levels of NRP2 were upregulated in HNC cohorts (n=57) compared to normal cohorts (n=31) from CPTAC. (D-E) Using GEO dataset (GSE30784 222877_at and 229225_at), the mRNA expression levels of NRP2 were upregulated compared to normal and dysplastic epithelium according to the development of the carcinogenesis. (F) The mRNA expression levels of NRP2 in 40 pairs of HNC tissues and adjacent normal epithelium tissues were analyzed by GEO dataset (GSE37991 ILMN_2376484).

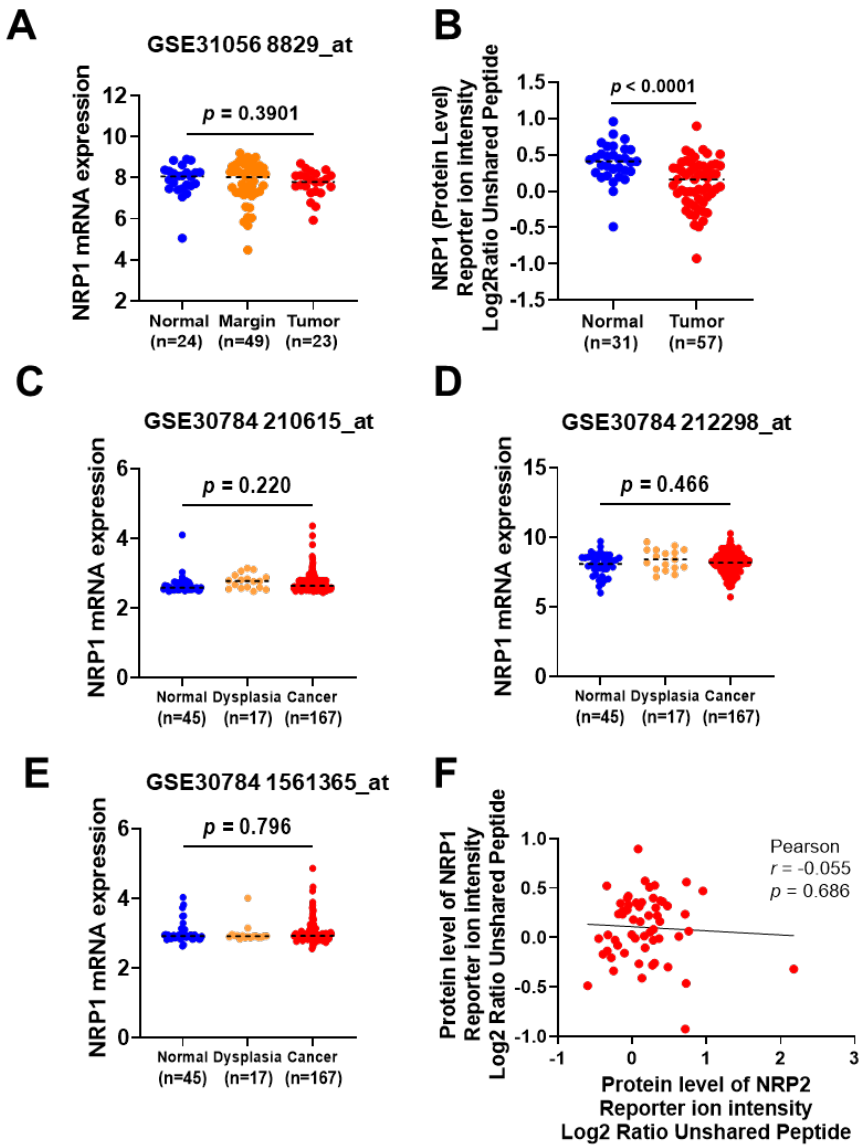

Figure 3. The expression NRP1 was analyzed in GEO and CTPAC.

(A) The mRNA expression levels of NRP1 were decreased in HNC in the comparison with normal and margin tissue from GEO dataset

(GSE31056). (B) The protein expression levels of NRP1 were decreased in HNC cohorts (n=57) compared to normal cohorts (n=31) from CPTAC. (C–E) Using GEO dataset (GSE30784 210615_at, 212298_at, and 1561365_at), the mRNA expression levels of NRP1 were shown little change compared to normal and dysplastic epithelium according to the development of the carcinogenesis. (F) A correlation between NRP2 and NRP1 protein levels was represented using CPTAC.

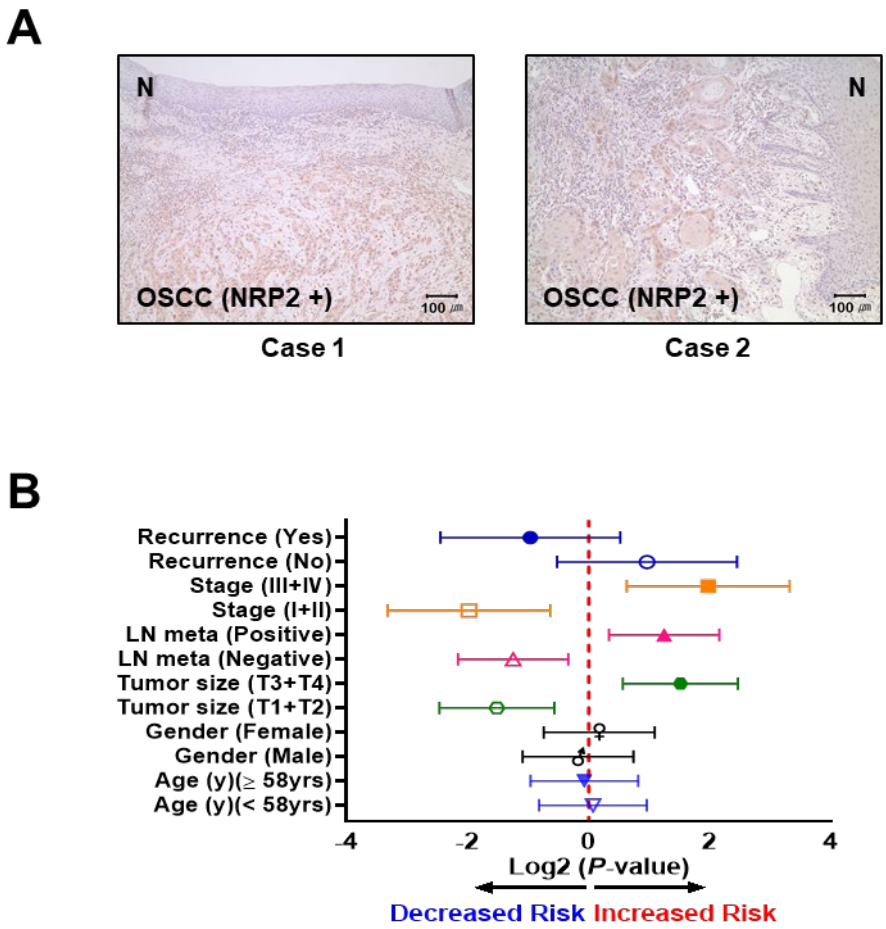

Figure 4. Clinicopathological features of NRP2 expression in OSCC tissues. (A) The expression level of NRP2 in OSCC tissues was detected by IHC analysis compared to the adjacent normal oral epithelium (N) (scale bar: 100 ㎛). (B) The representative graph showed the RR in clinicopathological features for NRP2.

Table 5. Relationship between NRP2 expression and clinicopathological factors in OSCC patients

Variable	No. of cases (N=53)	NRP2		*P*	Risk ratio	95 % CI
		Low (N=30)	High (N=23)			
Age						
<58	27	15	12	0.875	1.05	0.57−1.94
≥58	26	15	11		0.95	0.51−1.76
Gender						
Male	36	21	15	0.712	0.89	0.47−1.67
Female	17	9	8		1.13	0.60−2.13
Differentiation status						
Well	36	22	14	0.335	0.73	0.40−1.35
Moderately	17	8	9		1.36	0.74−2.50
Tumor size						
T1+T2	32	24	8	0.001*	0.35	0.18−0.68
T3+T4	21	6	15		2.86	1.48−5.52
LNM						
Negative	32	23	9	0.006*	0.42	0.22−0.79
Positive	21	7	14		2.37	1.26−4.46
Distant metastasis						
Negative	52	29	23	1.000	1.77	0.16−19.93
Positive	1	1	0		0.56	0.05−6.34
Stage						
I+II	24	20	4	< 0.001*	0.25	0.10−0.65
III+ IV	29	10	19		3.93	1.55−9.99
Recurrence						
No	41	21	20	0.144	1.95	0.70−5.46
Yes	12	9	3		0.51	0.18−1.43

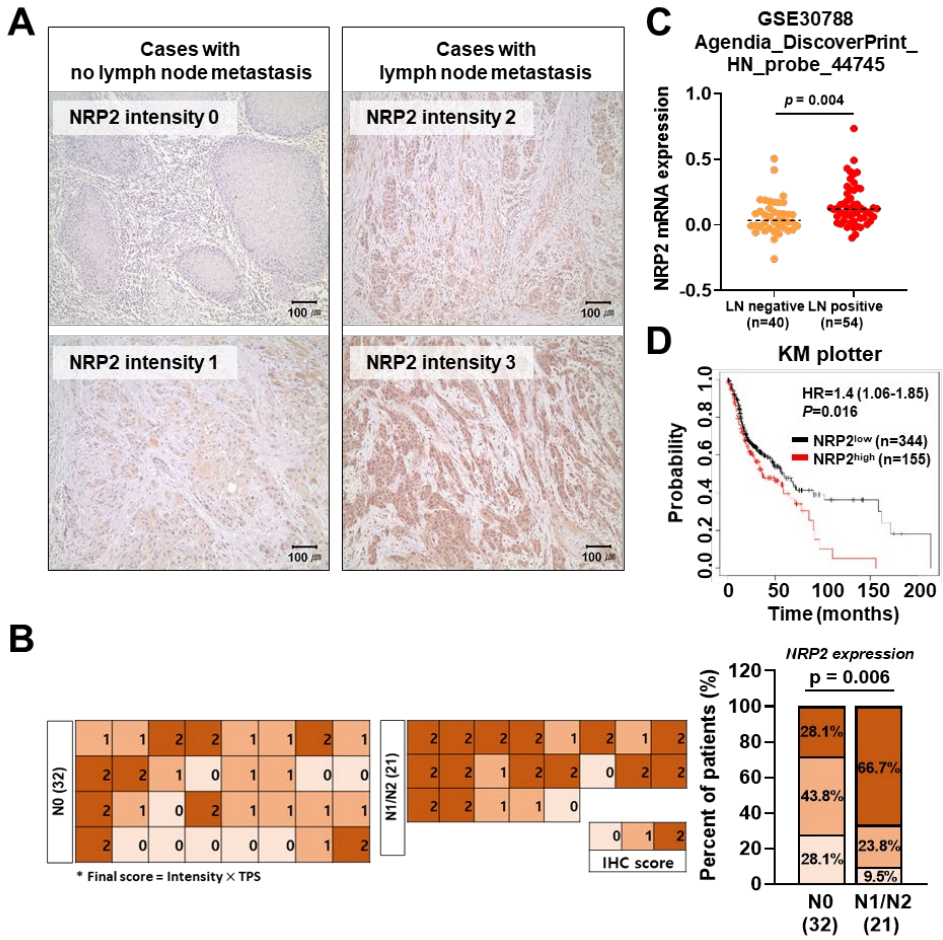

Figure 5. Association and prognosis between NRP2 expression and LNM in HNC patients. (A) The association between NRP2 intensity and LMN in 53 OSCC tissues was shown by IHC analysis (scale bar: 100 μm). (B) The graphical pattern was shown the corresponding IHC score of NRP2 expression in 53 OSCC tissues. (C) The mRNA

expression levels of NRP2 were upregulated in positive LNM cohorts (n=54) compared to negative LNM cohorts (n=40) from GEO dataset (GSE30788). (D) The expression level of NRP2 was significantly correlated with poor survival rate of HNC patients. KM plotter analysis showed that high NRP2 expression was associated with decreased OS rate for HNC cohort.

2. NRP2 promotes cell proliferation, motility, and invasiveness in human HNC.

To explore the functional role of NRP2 in HNC, I examined the expression levels of NRP2 in different HNC cell lines (FaDu, Ca9.22, HN22, HSC-2, HSC-3, HSC-4, MC-3, YD-15, and YD-15M) and normal HOK using immunoblotting. Protein expression levels of NRP2 were generally upregulated in various HNC cell lines except HSC-2 cell line compared to HOK (Figure 6A). Among these cell lines, I selected FaDu, HN22, and HSC-4 cell lines overexpressing NRP2 and constructed NRP2 knockdown stable cell lines with the expression vector of silencing NRP2. I then checked the expression of NRP2 between scramble and shNRP2 cell lines using RT-PCR and immunoblotting and found that the mRNA and protein expression levels of NRP2 were significantly downregulated in shNRP2 cell lines (Figure 6B and 6C).

Next, to determine whether NRP2 affects cell proliferation, I performed MTS assays in all three cell lines and confirmed that the cell viability of all shNRP2 cell lines was lower than scramble cell

lines at day 4 (Figure 7A). To evaluate whether NRP2 influences anchorage-independent growth abilities in HNC cell lines, soft agar assays were also performed following specific conditions of cell lines for 7 to 28 days. I counted the number of colonies greater than 50 μm and observed that knockdown of NRP2 induced significant decrease in that ability (Figure 7B). To confirm the effects of NRP2 on colony-forming abilities, I then performed a clonogenic assay in all NRP2 knockdown three stable cell lines and demonstrated that colony-forming abilities were decreased significantly in shNRP2 cell lines compared to scramble cell lines (Figure 7C). Interestingly, in an aspect of morphological features, the scramble cell lines were observed with aggressive mesenchymal phenotype in comparison with shNRP2 cell lines among all three cell lines (Figure 8A). To find out whether NRP2 affects cell motility and invasiveness, transwell migration assay and invasion assay were performed. I verified that knockdown of NRP2 inhibited migratory and invasive abilities in HNC cell lines (Figure 8B and 8C). All things considered, these results suggest that NRP2 promotes cell proliferation, motility, and invasiveness in human HNC.

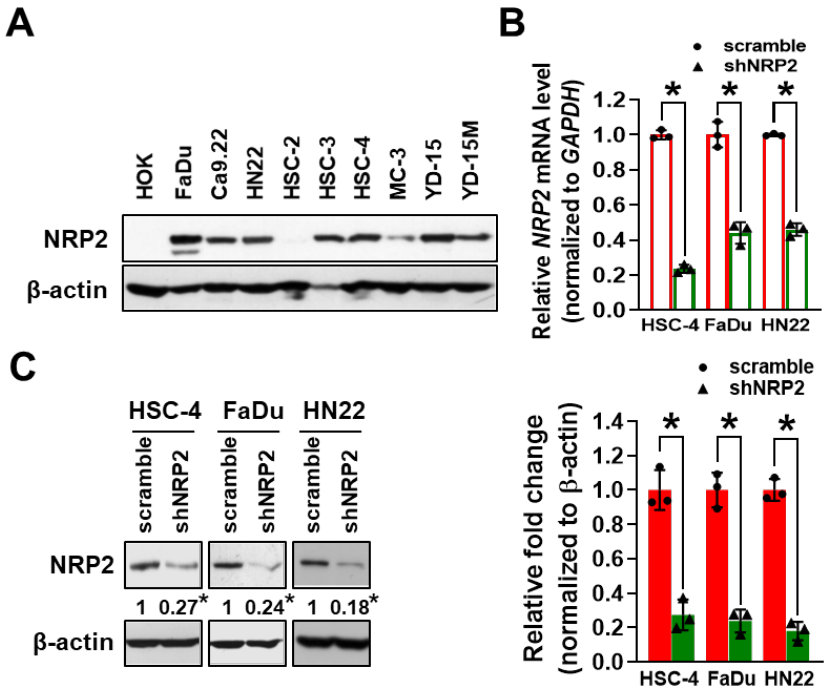

Figure 6. Construction to knockdown of NRP2 for stable HNC cell lines. (A) Immunoblotting images showing HNC cell lines and normal HOK to screen the expression of NRP2. (B) The mRNA expression levels of NRP2 in NRP2 knockdown three stable cell lines were determined by RT-PCR. *GAPDH* was used as the loading control. (C) Immunoblotting images showing NRP2 protein levels in NRP2 knockdown three stable cell lines. All results are expressed as mean ± standard deviation (SD) of three independent experiments. *P < 0.05 by two-tailed Student's t-test.

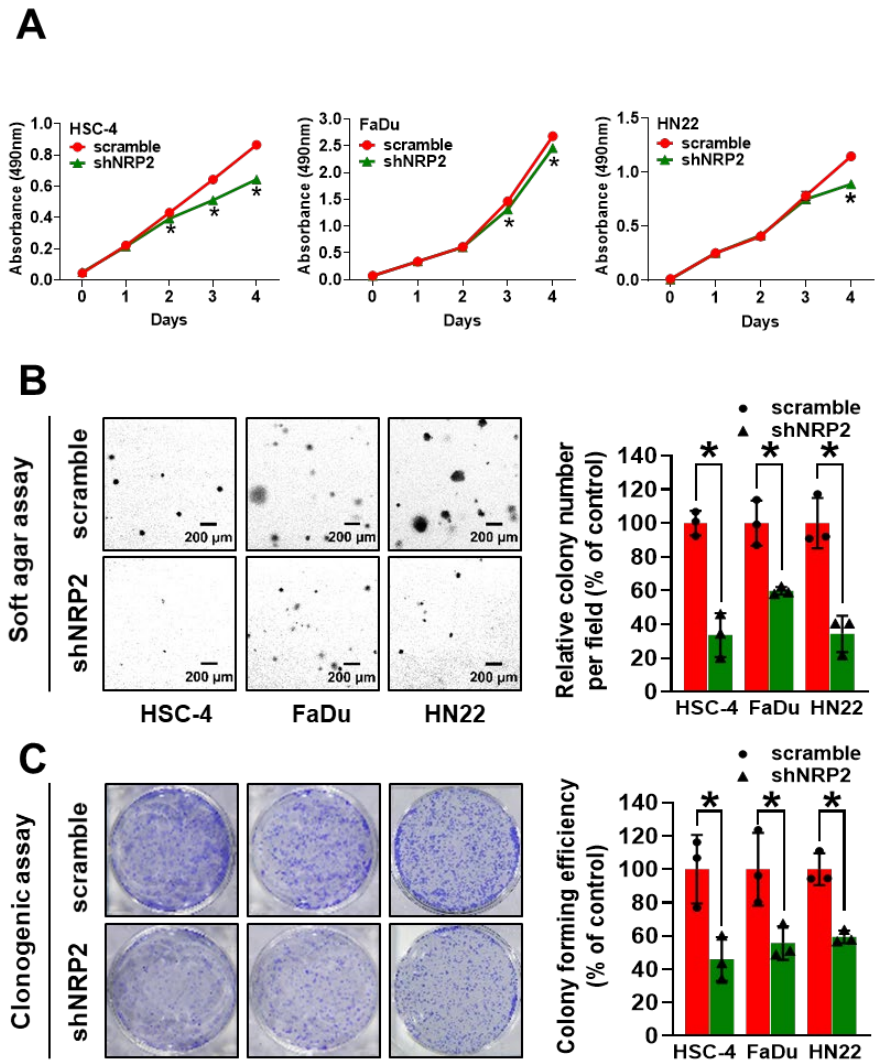

Figure 7. Functional role of NRP2 on cell proliferation. (A) Graphs showing the effect of cell viability in NRP2 knockdown three stable cell lines during 4 days using MTS assay. (B) Representative images

showing the anchorage-independent growth abilities using the soft agar assay in NRP2 knockdown three stable cell lines (scale bar: 200 μm). (C) Representative images showing the colony-forming efficiency using a clonogenic assay in NRP2 knockdown three stable cell lines. All graphs are represented as mean ± SD of three independent experiments. *P < 0.05 by two-tailed Student's t-test.

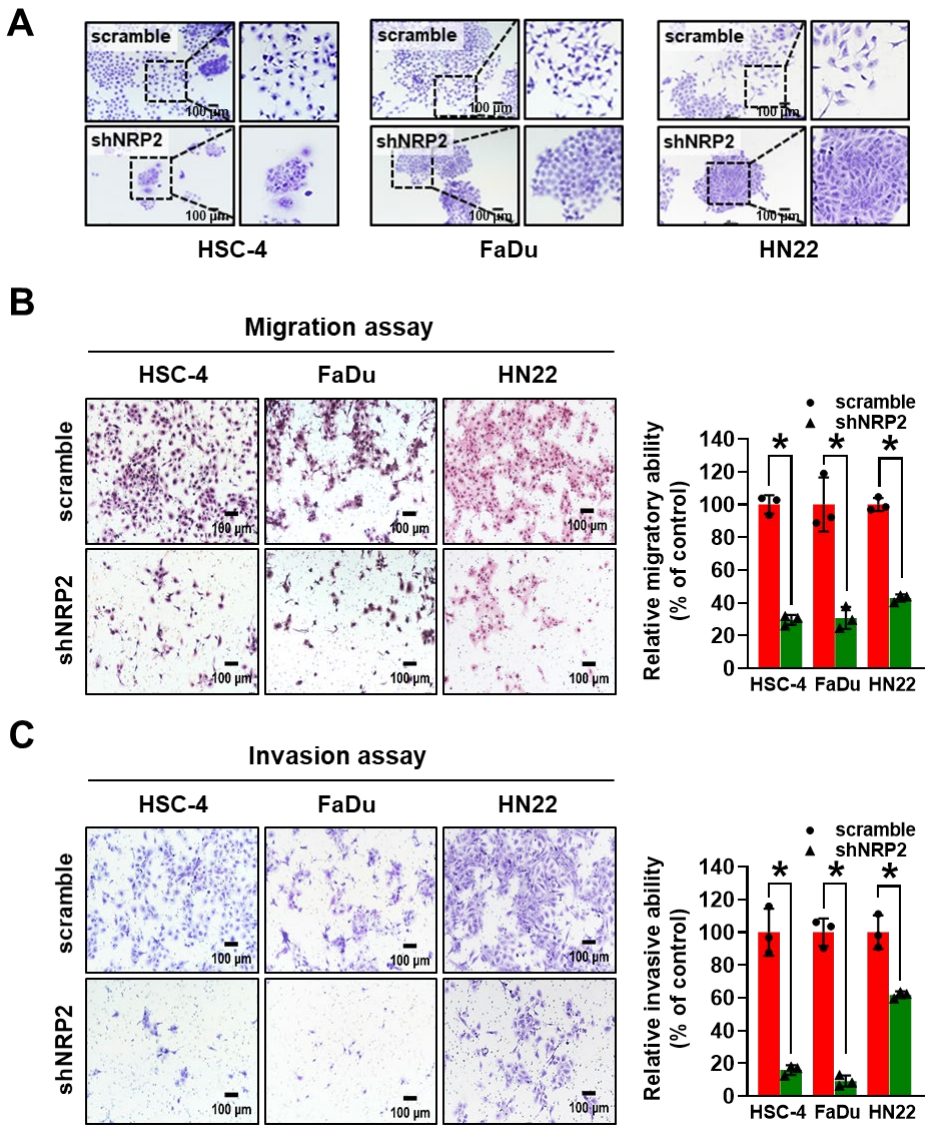

Figure 8. Effect of morphological features and the function of NRP2 on cell motility and invasiveness. (A) Representative images showing the observation of morphological features in NRP2 knockdown three

stable cell lines (scale bar: 100 μm). (B) Representative images showing the migratory ability between scramble and shNRP2 cell lines following the transwell migration assay (scale bar: 100 μm). (C) Representative images showing the invasive ability between scramble and shNRP2 cell lines following the Boyden chamber transwell invasion assay (scale bar: 100 μm). All graphs are expressed as mean ± SD of three independent experiments. *P < 0.05 by two-tailed Student's t-test.

3. Knockdown of NRP2 suppresses CSC properties by regulating Sox2 in HNC.

To identify the molecular downstream targets of NRP2 in HNC, I performed 1358 proteomic profiling of the NRP2 knockdown stable HSC-4 cell line. Of the 1,358 differentially expressed proteins with a fold change of more than 1.2 and p-value of less than 0.5 in the shNRP2 compared to scramble cells, 32 putative proteins were commonly extracted in two independent samples and were expressed by hierarchical clustering heatmap (Figure 9A). CSCs are defined as cells within the tumor that possess the self-renew capacity and give rise to a heterogeneous lineage of cancer cells (Clarke et al, 2006). It has been reported that the mRNA levels of CSC markers, BMI-1, Oct4, and Sox2, were elevated when NRP2 was overexpressed in breast cancer (Goel et al, 2013). It was also reported that CD44 as a CSC marker is overexpressed in most oral cancer cell lines and Oct3/4 and Sox2 which are specifically expressed in progenitor cells and stem cells are overexpressed in the HSC-4 cell line (Noto et al, 2013). In accordance with the hierarchical clustering heatmap, I

selected Sox2 as a downstream molecule among several candidate molecules and confirmed the protein expression of Sox2 in both NRP2 knockdown stable HSC-4 and FaDu cell lines using immunoblotting. Surprisingly, I found that protein expression levels of Sox2 in shNRP2 cell lines were downregulated compared with the corresponding scramble cell lines (Figure 9B). I further confirmed that Pearson's correlation between NRP2 and Sox2 protein levels was positive using CPTAC ($r = 0.278$, $p = 0.04$, Figure 9C).

Recently, several studies have demonstrated that the expression of Sox2 is associated with metastasis and stemness (Ren et al, 2016). To explore the biological function of Sox2, the HSC-4 and FaDu cell lines were transfected and then knocked down by adapting siSox2 (40 nM). I confirmed that the protein expression levels of Sox2 in siSox2-transfected cells remarkably decreased compared to sicontrol cells using immunoblotting (Figure 10A). Further, to test whether siSox2 was able to affect both migratory and invasive abilities in human HNC cell lines, I performed the transient transfection using siSox2 and then evaluated migration or invasion assay in both HSC-4 and FaDu cell lines. Consistent with the results

from the NRP2 knockdown stable cell lines, transient knockdown of Sox2 suppressed the migratory and invasive abilities in both cell lines (Figure 10B and 10C). To further investigate the protein expression levels of Nanog and Oct4, which are representative CSC markers, I checked the protein levels of Nanog and Oct4 in both NRP2 knockdown stable cell lines. The protein expression levels of Nanog were significantly decreased in both NRP2 knockdown stable cell lines, whereas Oct4 was inconsistent in two cell lines (Figure 11A). Next, *in vitro*, sphere formation assay has been used to identify the capacity of differentiation and self-renewal in stem cells and CSCs (Clarke et al, 2006). I found that sphere-forming abilities were decreased in both NRP2 knockdown stable HSC-4 and FaDu cell lines (Figure 11B). These results demonstrated that knockdown of NRP2 may suppress CSC properties by dominantly regulating Sox2 in human HNC cell lines.

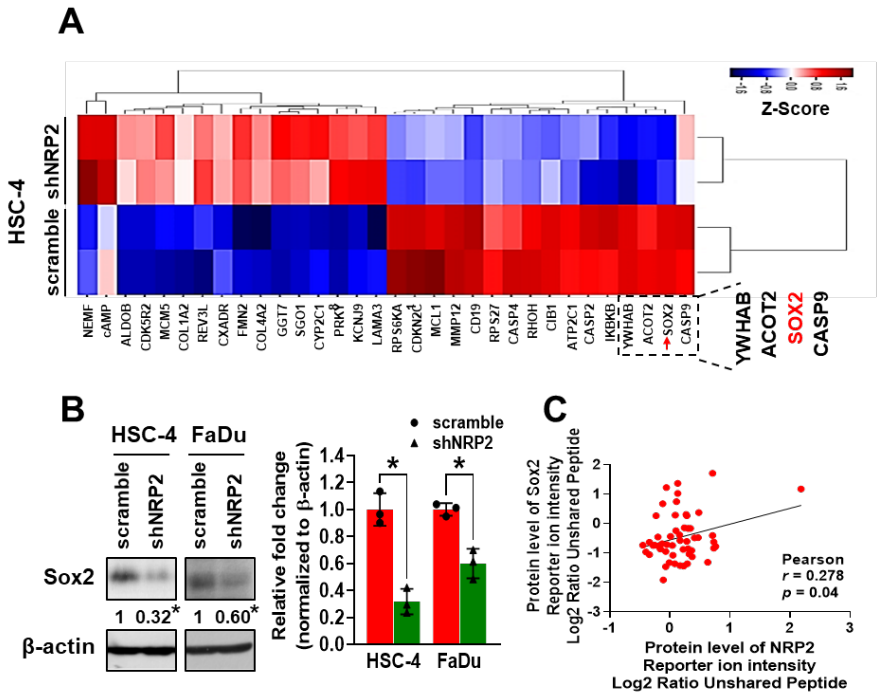

Figure 9. Exploring the downstream molecules of NRP2 through protein profiling. (A) Hierarchical clustering heatmap showing differential expression of 32 proteins among 1358 proteins. The criteria of extracted proteins are fold-change > 1.2 and p-value < 0.05. (B) Immunoblotting images showing the protein expression levels of Sox2 in both NRP2 knockdown stable HSC-4 and FaDu cell lines. The graph is represented as mean ± SD of three independent experiments. *P < 0.05 by two-tailed Student's t-test. (C) A positive correlation between NRP2 and Sox2 protein levels was represented using CPTAC.

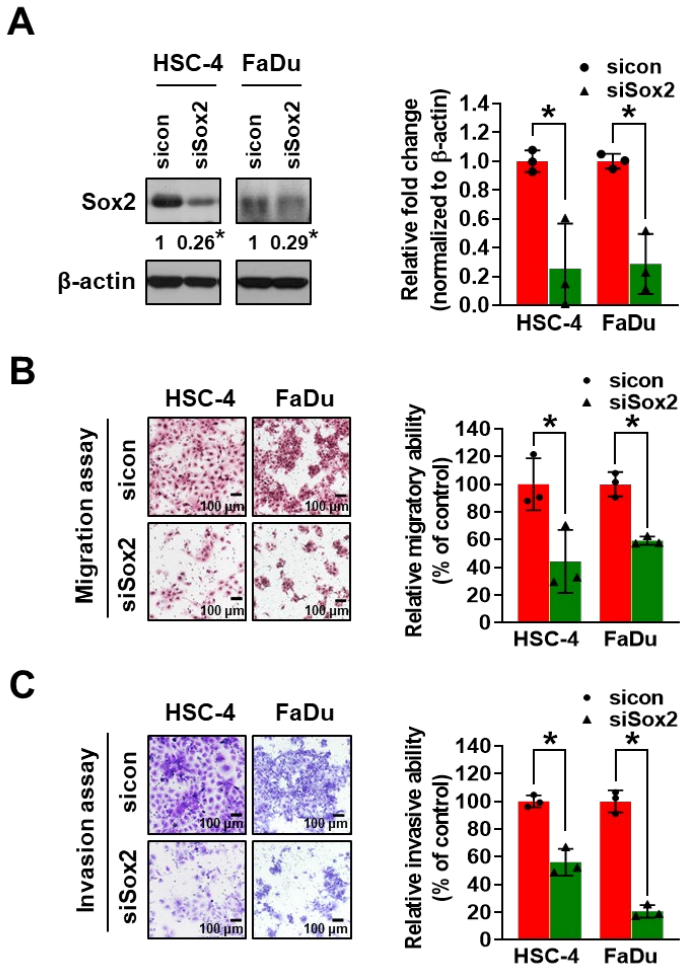

Figure 10. The role of Sox2 as a downstream molecule of NRP2 to cell motility and invasiveness. (A) Immunoblotting images showing the protein expression levels of Sox2 between sicontrol and siSox2 transfected cells in HSC−4 and FaDu cell lines. (B) Representative images showing the migratory ability between sicontrol cells and siSox2 transfected cells following the transwell migration assay

(scale bar: 100 μm). (C) Representative images showing the invasive ability between sicontrol and siSox2 transfected cells following the Boyden chamber transwell invasion assay (scale bar: 100 μm). All graphs are represented as mean $\pm$ SD of three independent experiments. *P < 0.05 by two-tailed Student's t-test.

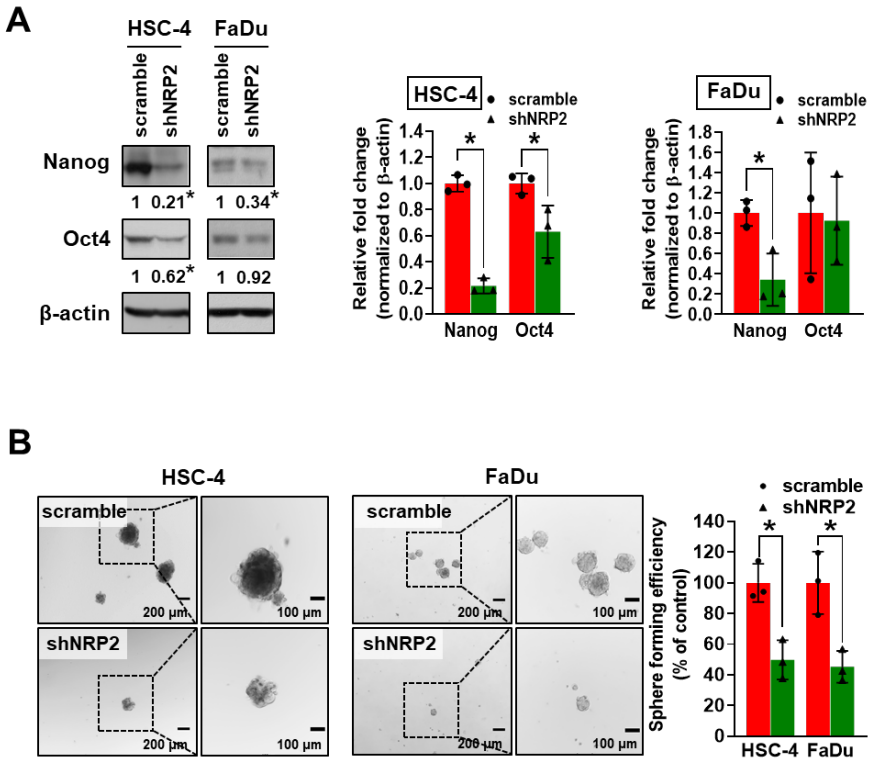

Figure 11. Relevance between NRP2 and CSC properties. (A) Immunoblotting images showing the protein expression levels of CSC markers, Nanog and Oct4, in both NRP2 knockdown stable HSC-4 and FaDu cell lines. (B) Representative images showing the sphere-forming efficiency in both NRP2 knockdown stable HSC-4 and FaDu cell lines (scale bar: 100 and 200 μm). All data are expressed as mean ± SD of three independent experiments. *P < 0.05 by two-tailed Student's t-test.

4. RSK1 is mediated between NRP2 and Sox2.

To further identify the underlying mechanism of the NRP2 signaling pathway, I tried to search which kinase mediates between NRP2 and Sox2 among protein kinase candidates according to protein profiling. As previously reported (Kang et al, 2010, Li et al, 2020), RSK2 promoted metastasis in HNC and RSK4 regulated CSC properties in esophageal SCC. In accordance with 1,358 protein profiling, 5 ribosomal protein kinases including RPS6KA1 (RSK1), RPS6KA2 (RSK3), RPS6KA6 (RSK4), RPS6KB1 (p70S6Kα), and MSP1 were expressed by hierarchical clustering heatmap (Figure 12A). Interestingly, only the RPS6KA1 was statistically significant (fold change = 0.56, p = 0.020), whereas RPS6KA2, RPS6KA6, and RPS6KB1 showed inconsistent patterns. I investigated the protein expression levels of p-p90RSK$^{(T359/S363)}$ and RSK1 in both NRP2 knockdown stable HSC-4 and FaDu cell lines using immunoblotting and found that p-p90RSK$^{(T359/S363)}$ and RSK1 were consistently downregulated corresponding to the knockdown of NRP2 (Figure 12B).

To confirm whether RSK1 can regulate Sox2, I used a RSK inhibitor BI-D1870, which acts as a reversible ATP-competitive inhibitor of the N-terminal kinase domain of RSKs (Romeo et al, 2012). I first examined the toxicity of BI-D1870 on HSC-4 and FaDu lines using the trypan blue exclusion assay and found relevant concentrations (0.8 μM for HSC-4 and 1 μM for FaDu) minimally inducing cytotoxicity between vehicle (DMSO) and BI-D1870-treated groups (Figure 13A). I then performed immunoblotting on both HSC-4 and FaDu cell lines and verified that the BI-D1870 remarkably reduced the expression levels of Sox2 in both HSC-4 and FaDu cell lines (Figure 13B). I next demonstrated whether suppression of RSK1 by BI-D1870 may influence the migratory or invasive ability in both HSC-4 and FaDu cell lines. As shown in Figure 14A and 14B, BI-D1870 diminished HNC cell migratory and invasive abilities. These results indicate that downregulation of RSK1/Sox2 axis may inhibit cell motility and invasiveness. To further find the relation between RSK1 and CSC properties, I examined the expression of CSC markers and sphere-forming efficiency using immunoblotting and sphere formation assay after treatment of BI-

1870 in both HSC-4 and FaDu cell lines, respectively. The protein expression levels of Nanog were significantly decreased after treating BI-D1870 in both cell lines, whereas the expression of Oct4 was not significantly changed (Figure 15A). As shown in Figure 15B, sphere formation efficiency was noticeably reduced with a BI-D1870. These results indicate that RSK1 also may modulate cell migratory, invasive abilities, and CSC properties in human HNC cell lines.

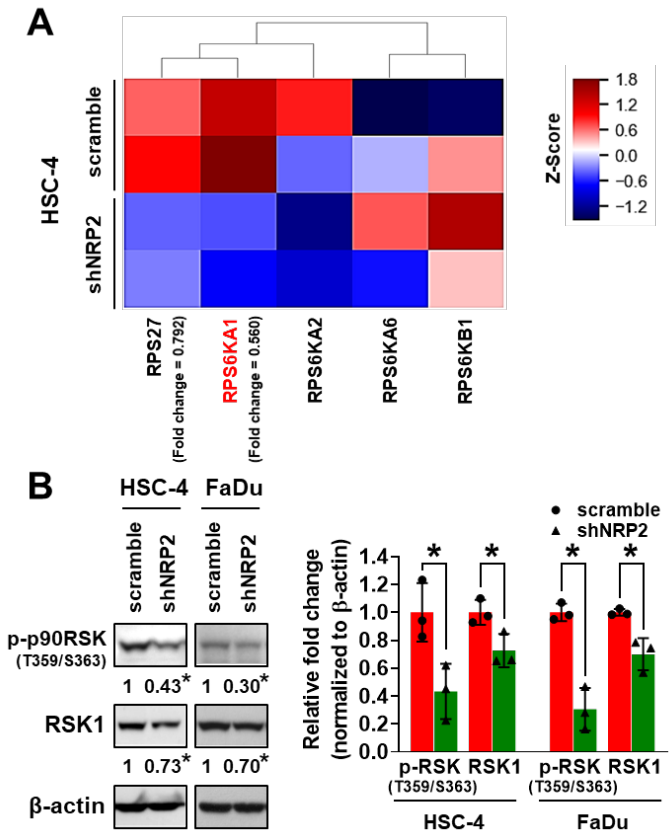

Figure 12. Searching for a kinase that connects NRP2 and Sox2. (A) Hierarchical clustering heatmap showing differential expression of 5 proteins related in ribosomal kinases. (B) Immunoblotting images showing the protein expression levels of p-p90RSK $^{(T359/S363)}$ and RSK1 in both NRP2 knockdown stable HSC-4 and FaDu cell lines. The graph is represented as mean ± SD of three independent experiments. *P < 0.05 by two-tailed Student's t-test.

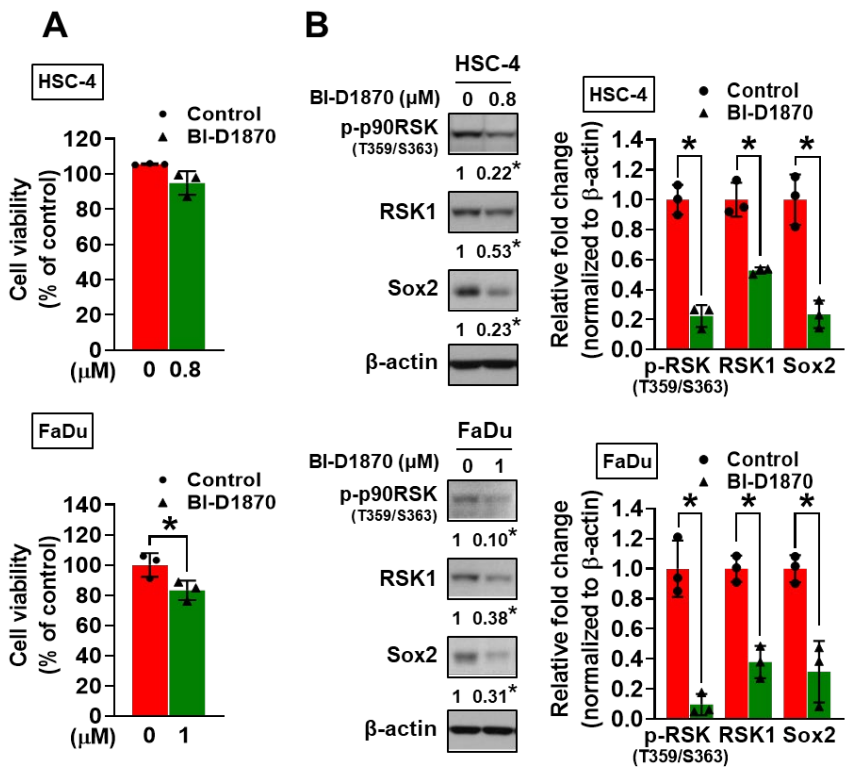

Figure 13. Regulatory mechanism of the BI-D1870. (A) HSC-4 and FaDu cell lines were treated with DMSO or the doses of BI-D1870 (0.8 μM for HSC-4 and 1 μM for FaDu). Cell viability was evaluated by the trypan blue exclusive assay. (B) Immunoblotting images showing the protein expression levels of p-p90RSK/RSK1/Sox2 axis with the treatment of DMSO or BI-D1870 in both HSC-4 and FaDu cell lines. All data are represented as mean ± SD of three independent experiments. *P < 0.05 by two-tailed Student's t-test.

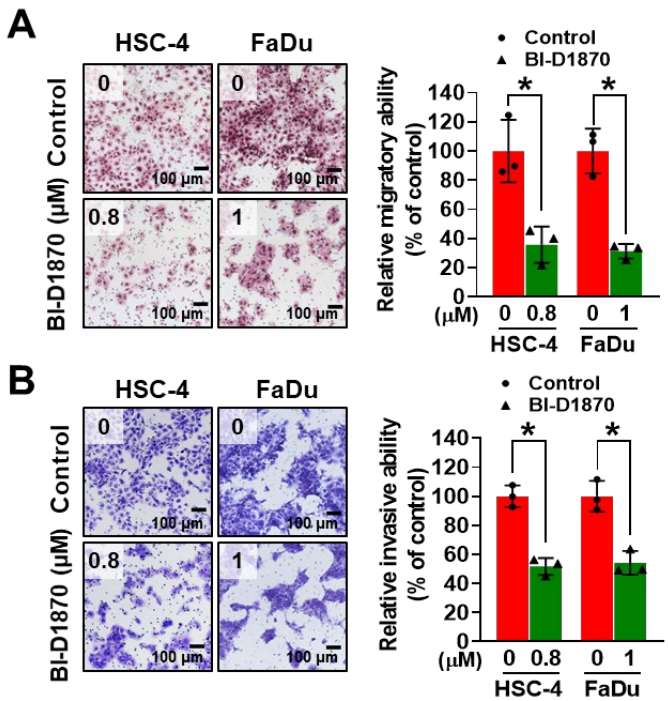

Figure 14. Association between BI-D1870 and cell motility and invasiveness. (A) Representative images showing the migratory ability between treated with DMSO and BI-D1870 (0.8 μM for HSC-4 and 1 μM for FaDu) following the transwell migration assay (scale bar: 100 μm). (B) Representative images showing the invasive ability between treated with DMSO and BI-D1870 following the Boyden chamber transwell invasion assay (scale bar: 100 μm). All graphs are represented as mean ± SD of three independent experiments. *P < 0.05 by two-tailed Student's t-test.

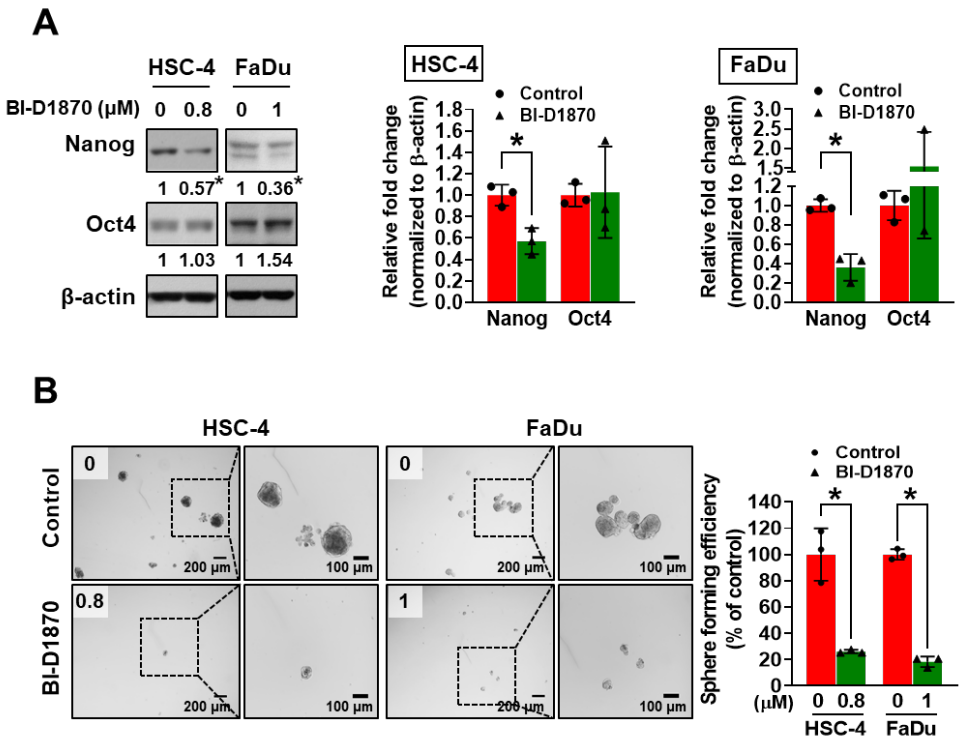

Figure 15. Correlation between BI-D1870 and CSC properties. (A) Immunoblotting images showing the protein expression levels of CSC markers, Nanog and Oct4, between treated with DMSO and BI-D1870 (0.8 μM for HSC-4 and 1 μM for FaDu) in both HSC-4 and FaDu cell lines. (B) Representative images showing the sphere-forming efficiency between treated with DMSO and BI-D1870 in both cell lines (scale bar: 100 and 200 μm). All data are expressed as mean ± SD of three independent experiments. *P < 0.05 by two-tailed Student's t-test.

5. NRP2 is required for HNC metastatic events.

I constructed a pBabe puro-based retroviral vector for overexpression of NRP2 in HSC-2 cell line which had low expression of NRP2 among HNC cell lines and attempted to clarify the underlying mechanism of NRP2. The results showed that the expression levels of p-p90RSK$^{(T359/S363)}$, RSK1, and Sox2 were significantly upregulated when NRP2 was overexpressed (Figure 16A). I also found that overexpression of NRP2 decreased the number of colonies and clusters (Figure 16B and 16C) and significantly enhanced migratory and invasive abilities in NRP2 O/E stable HSC-2 cell lines (Figure 17A). In addition, I demonstrated that tumor-sphere forming efficiency was significantly increased as the protein expression level of Nanog was increased in NRP2 O/E stable HSC-2 cell lines (Figure 17B and 17C). The results suggest that NRP2 is associated with migration, invasion, and CSC properties in human HNC.

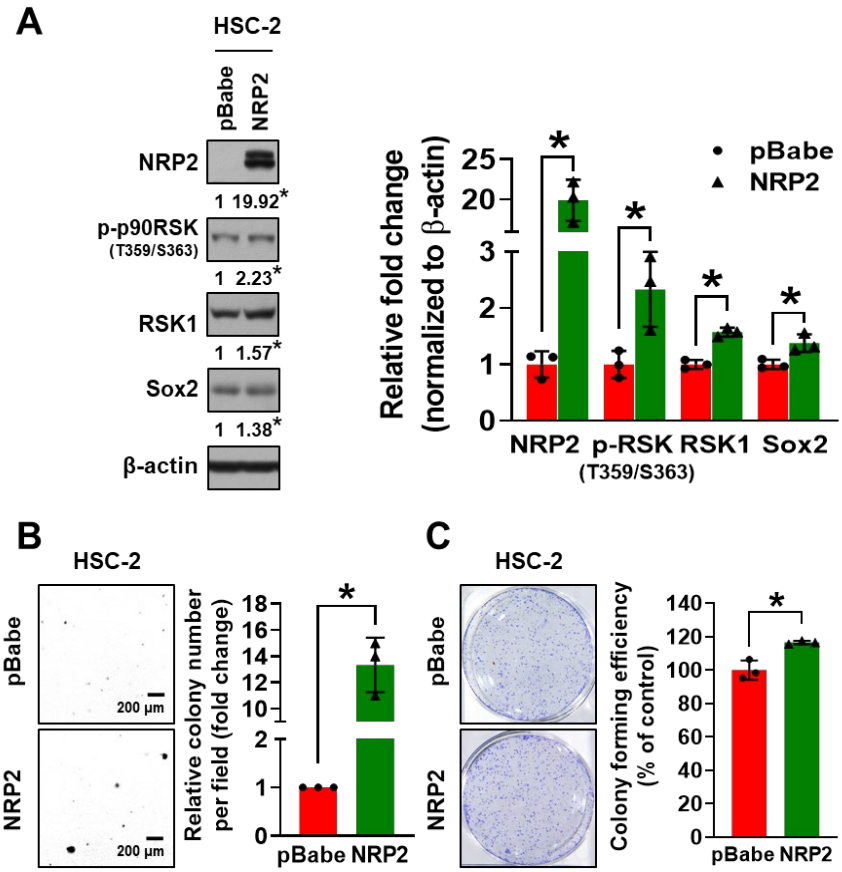

Figure 16. Confirmation of NRP2 mechanism in NRP2 O/E stable HSC-2 cell lines. (A) Immunoblotting images showing the protein expression levels of downstream molecules of the NRP2 signaling in NRP2 O/E stable HSC-2 cell lines. (B) Representative images showing the anchorage-independent growth ability using the soft agar assay in NRP2 O/E stable HSC-2 cell line (scale bar: 200 μm).

(C) Representative images showing the colony-forming efficiency using a clonogenic assay in NRP2 O/E stable HSC-2. All data are represented as mean ± SD of three independent experiments. *P < 0.05 by two-tailed Student's t-test.

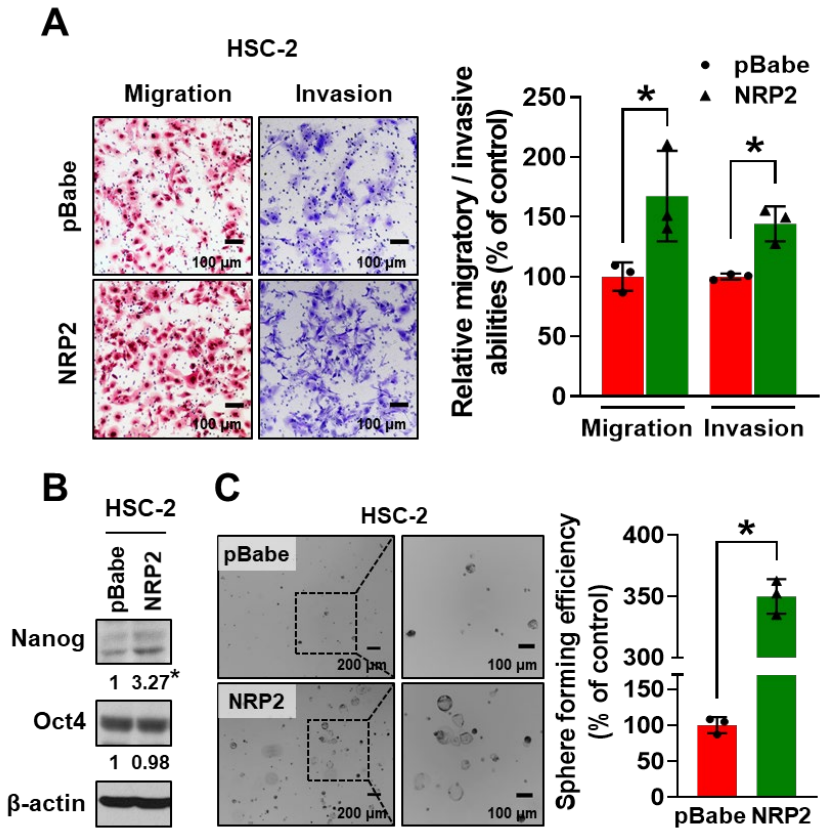

Figure 17. Analysis of the functional roles of NRP2 in the NRP2 O/E stable HSC-2 cell lines. (A) Representative images showing the migratory and invasive abilities between pBabe and NRP2 O/E cell lines following transwell assay (scale bar: 100 μm). (B) Immunoblotting images showing the protein expression levels of Nanog and Oct4 in NRP2 O/E stable HSC-2 cell line. (C) Representative images showing the sphere-forming efficiency in

NRP2 O/E stable HSC-2 cell lines (scale bar: 100 and 200 μm). All data are expressed as mean ± SD of three independent experiments. *P < 0.05 by two-tailed Student's t-test.

6. The key EMT marker that regulates cell motility and invasiveness is Zeb1 through the NRP2/RSK1/Sox2 pathway.

EMT is a crucial process that transforms adherent epithelial cells into mesenchymal cells, enabling the extracellular matrix to degrade and migrate (Welch and Hurst, 2019). The morphological feature of invasive cells shows non-polarized, fibroblast-like, and spindle-like morphology. To determine which EMT markers (Zeb1, Zeb2, Slug, Twist, Fibronectin, ZO-1 and E-cadherin) regulate cell motility and invasiveness through NRP2/RSK1/Sox2 axis in HNC cell lines, I screened EMT markers in NRP2 knockdown stable HSC-4 and FaDu cell lines using immunoblotting and found that regulatory EMT markers were Zeb1 and E-cadherin (Figure 18A). To further explore the relevance of EMT with Sox2 and RSK, siSox2 or BI-D1870 were used. I demonstrated that the protein expression of Zeb1 was commonly decreased in both HSC-4 and FaDu cell lines (Figure 18B and 18C). Contrastively, the protein expression of Zeb1 was increased in NRP2 O/E stable HSC-2 cell line (Figure 18D). The protein expression levels of E-cadherin were inconsistent. These

results suggest that the key EMT marker that regulates cell motility and invasiveness may be Zeb1 through the NRP2/RSK1/Sox2 pathway.

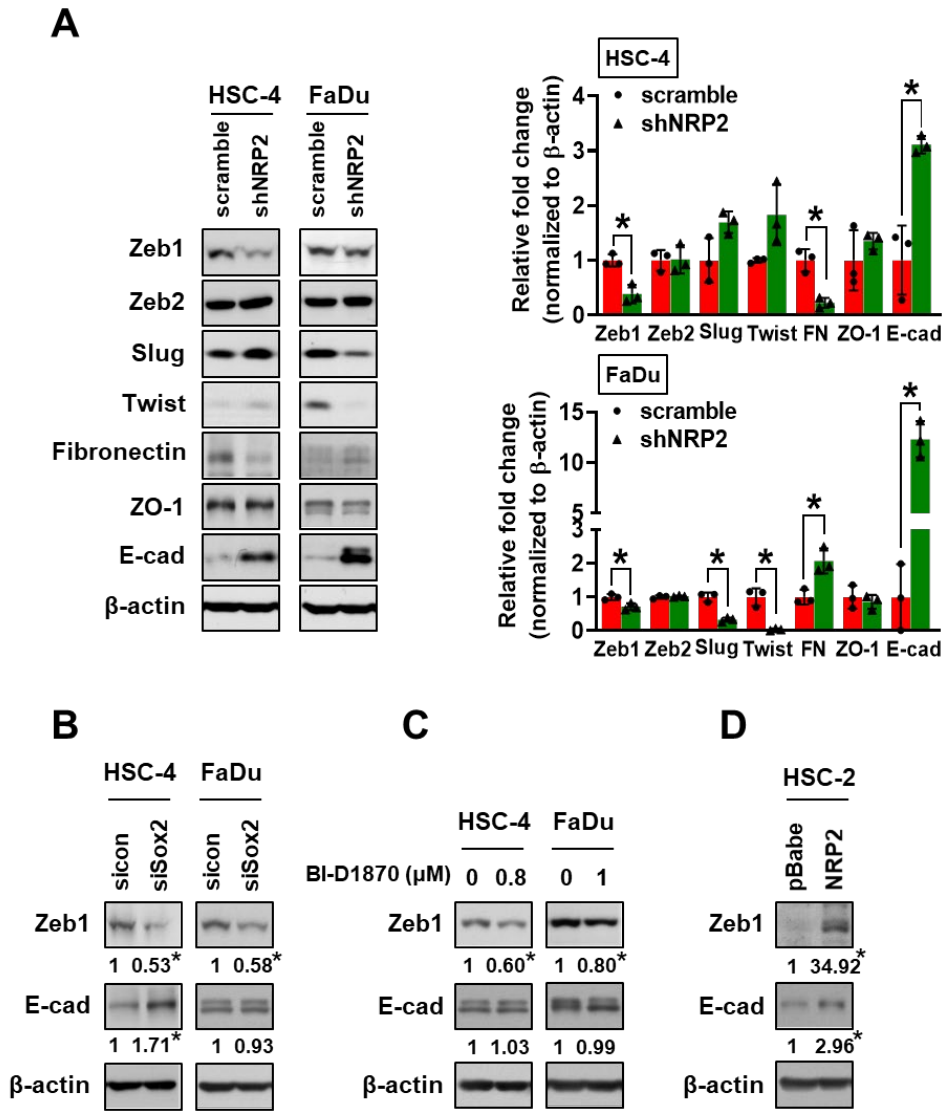

Figure 18. Screening for commonly regulated EMT markers. (A) Immunoblotting images showing the screening of protein expression levels of EMT markers in both NRP2 knockdown stable HSC-4 and

FaDu cell lines. (B) Immunoblotting images showing the protein expression levels of Zeb1 and E-cadherin between transfected sicontrol and siSox2 cells. (C) Immunoblotting images showing the protein expression levels of Zeb1 and E-cadherin between treated with DMSO and BI-D1870 (0.8 μM for HSC-4 and 1 μM for FaDu) in both HSC-4 and FaDu cell lines. (D) Immunoblotting images showing the protein expression levels of Zeb1 and E-cadherin in NRP2 O/E stable HSC-2 cell line. All data are expressed as mean $\pm$ SD of three independent experiments. *P < 0.05 by two-tailed Student's t-test.

7. MECF may comply with the NRP2/RSK1/Sox2 axis in human HNC.

To explore a marine resource that has potential as natural chemotherapeutic agents targeting NRP2 in HNC, the methanol extracts of 20 species of marine algae were screened. The information of species names for 20 marine algae was listed in Table 1. I first evaluated that 20 kinds of methanol extracts were treated on the HSC-4 cell line at a concentration of 20 μg/ml for MTS assay. The results showed that cell viability was not affected after 48 h (Figure 19A and Table 1). I then checked the protein expression levels of NRP2 using immunoblotting. The results showed that only No. 17, MECF remarkably downregulated NRP2 protein levels in HSC-4 cell line (Figure 19B). Consistent with the the results of MTS assay, MECF treatment at the concentration of 20 μg/ml did not show noticeable cytotoxicity using the trypan exclusion assay in HSC-4, FaDu, and HN22 cell lines (Figure 19C). I also observed that the protein expression levels of NRP2 were markedly reduced when three cell lines were treated with the same corresponding concentration of MECF (Figure 19D).

To determine whether MECF regulates cell motility and invasiveness in HNC cell lines, I performed migration and invasion assays in three cell lines. The results showed that migratory and invasive abilities were strongly decreased with MECF treatment in both HSC-4 and HN22 cell lines, whereas FaDu cells were suppressed only in the invasion assay without affecting their migratory ability after MECF treatment (Figure 20A and 20B). To identify whether MECF may regulate downstream substrates of NRP2, I performed immunoblotting to detect the protein levels of p-p90RSK$^{(T359/S363)}$, RSK1, Sox2, and Zeb1 in three cell lines. As expected, the results showed that the protein expression levels of downstream substrates, p-p90RSK$^{(T359/S363)}$, RSK1, Sox2, and Zeb1, were significantly decreased in three cell lines (Figure 21). At the same concentration of MECF, the protein expression levels of Nanog and Oct4 were also downregulated in both HSC-4 and FaDu cell lines (Figure 22A). To investigate whether MECF may regulate CSC properties, I conducted the sphere formation assay in both HSC-4 and FaDu cell lines and found that MECF disrupted CSC properties not by forming any tumorspheres (Figure 22B). These results

suggest that MECF may appear to exert anti-migratory, invasive, and sphere-forming activities by conforming to the NRP2/RSK1/Sox2 axis in human HNC cell lines.

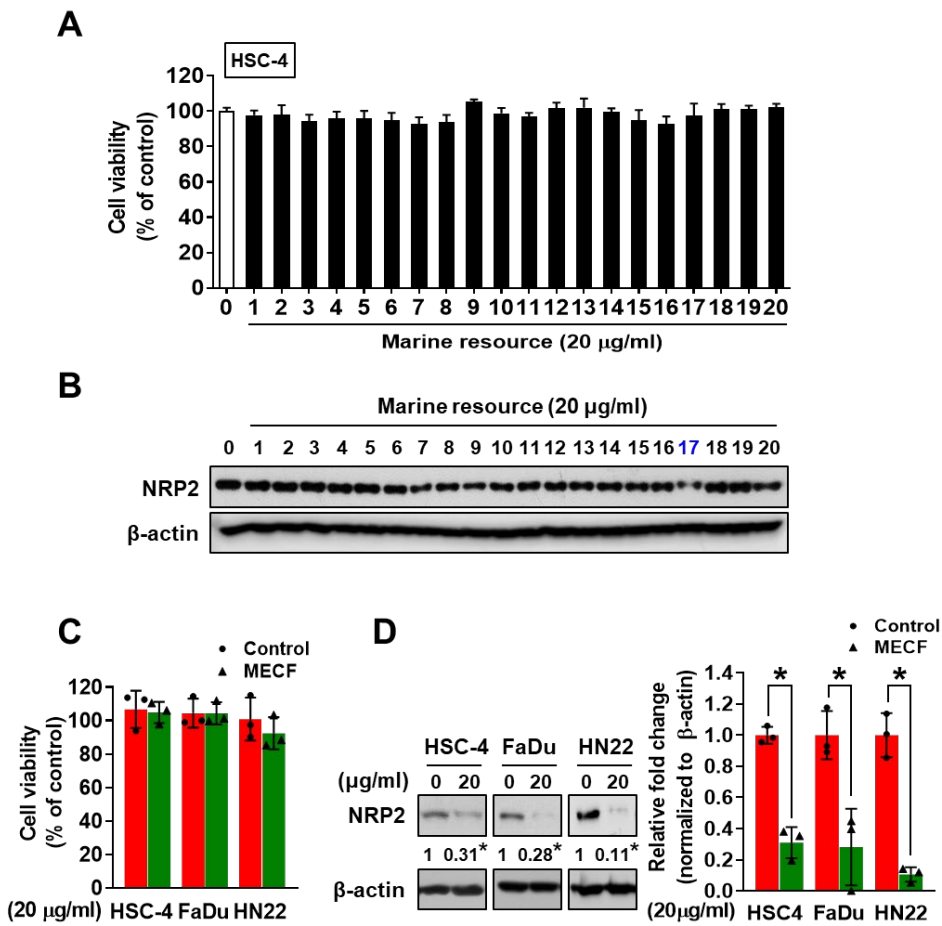

Figure 19. Exploration of 20 marine resource extracts for targeting NRP2. (A) Cytotoxicity with the treatment of methanol extracts of 20 marine resources at the concentration of 20 μg/ml was evaluated by MTS assay in HSC-4 cell line. The graph was represented as mean ± SD of five independent experiments. (B) Immunoblotting was performed to screen 20 kinds of marine resource extracts for

targeting NRP2. (C) MECF at the concentration of 20 μg/ml was treated in HSC-4, FaDu, and HN22 cell lines. Cell viability was evaluated by the trypan blue exclusive assay. (D) Immunoblotting images showing the protein expression levels of NRP2 with the treatment of MECF at the concentration of 20 μg/ml in three cell lines. The data are represented as mean $\pm$ SD of three independent experiments. *P < 0.05 by two-tailed Student's t-test.

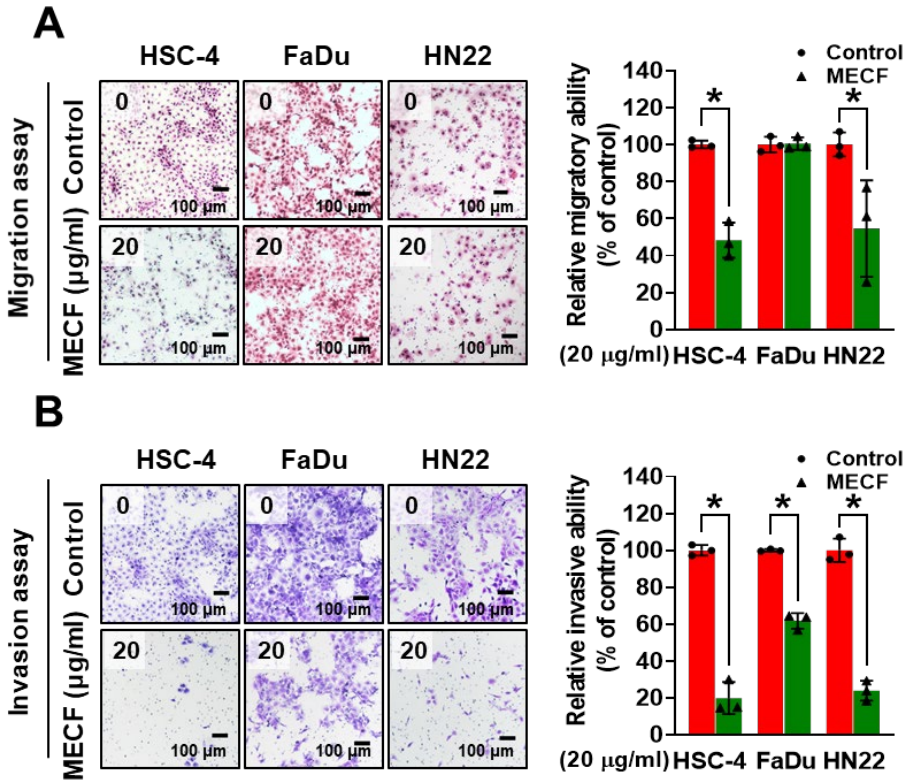

Figure 20. Evaluation of the efficacy of cell motility and invasiveness by treating MECF. (A) Representative images showing the migratory ability between treated with DMSO and MECF following the transwell migration assay (scale bar: 100 μm). (B) Representative images showing the invasive ability between treated with DMSO and MECF following the Boyden chamber transwell invasion assay (scale bar: 100 μm). All graphs are represented as mean ± SD of three independent experiments. *P < 0.05 by two-tailed Student's t-test.

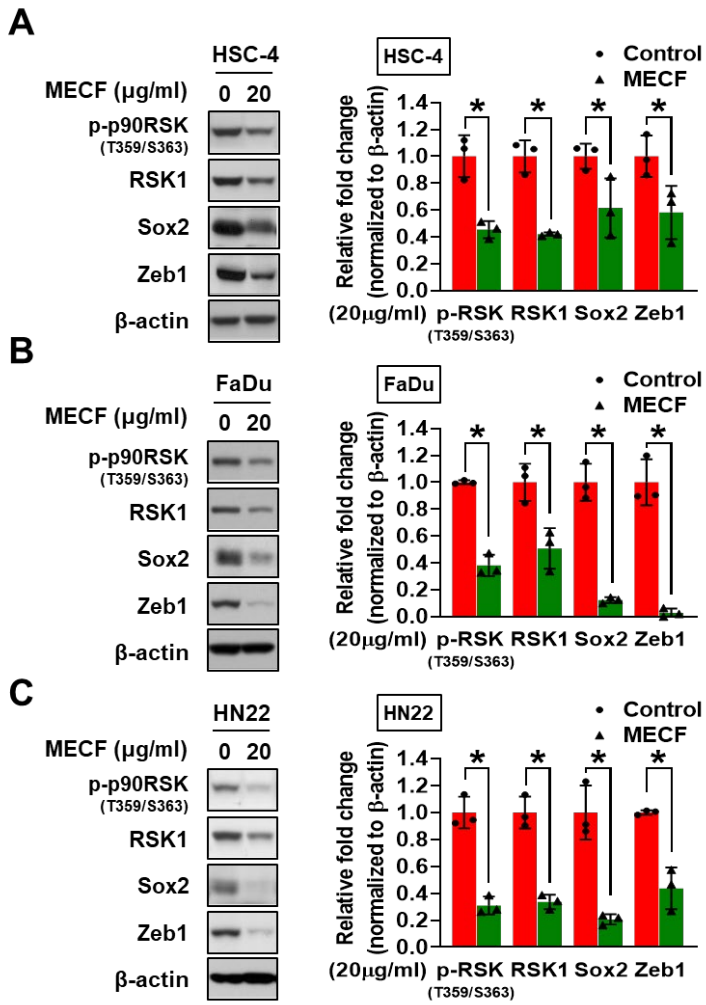

Figure 21. Confirmation of the mechanism controlled by the MECF in HNC cell lines. (A–C) Immunoblotting images showing the protein expression levels of downstream molecules of the NRP2 signaling with the treatment DMSO or MECF in HSC–4, FaDu, and HN22 cell lines. All data are expressed as mean ± SD of three independent experiments. *P < 0.05 by two–tailed Student's t–test.

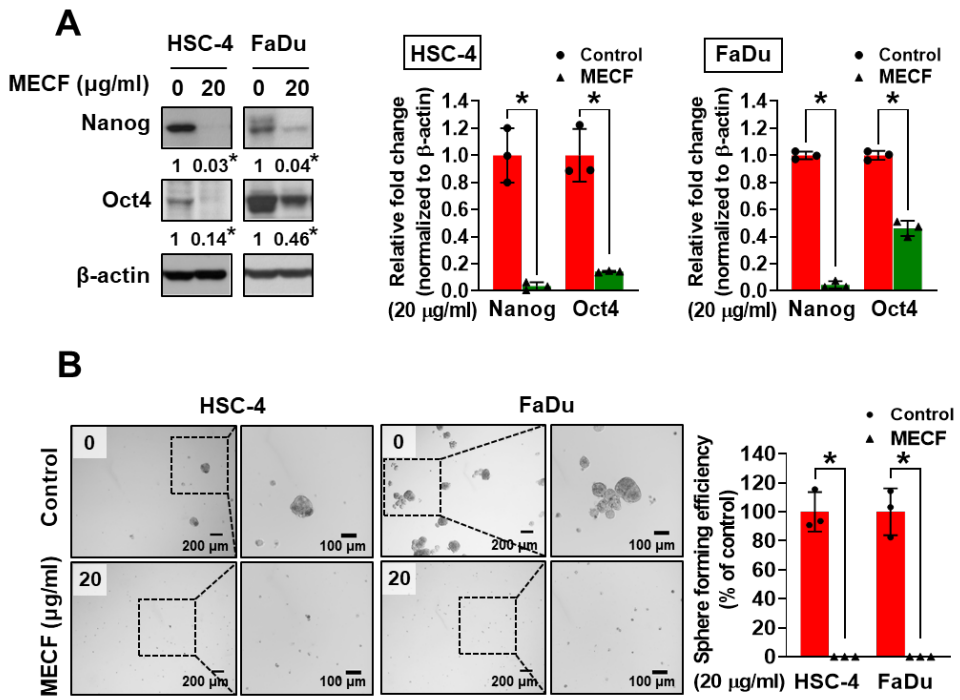

Figure 22. Effect of MECF on CSC properties by regulating NRP2 pathway. (A) Immunoblotting images showing the protein expression levels of CSC markers, Nanog and Oct4, between treated with DMSO and MECF in both HSC-4 and FaDu cell lines. (B) Representative images showing the sphere-forming efficiency between treated with DMSO and MECF in both cell lines (scale bar: 100 and 200 μm). All data are expressed as mean ± SD of three independent experiments. *P < 0.05 by two-tailed Student's t-test.

8. The expression of VEGFR-1/3 was associated with NRP2 in HNC.

To determine whether the expression of VEGFRs was related to NRP2 in HNC, I analyzed the correlation between mRNA or protein expression levels of VEGFRs and NRP2 *in silico*. The results showed that the association between mRNA expression levels of VEGFR-1/3 and NRP2 in OSCC tissues (n=167) was positively correlated (Figure 23A and 23C), but VEGFR-2 was not significant (Figure 23B). Using CPTAC, the protein expression levels of VEGFR-1 were also correlated with NRP2 in HNC tissues (n=57) (Figure 23D). These results indicated that the overexpressed NRP2 may evoke a metastatic signaling pathway by positively correlating with the expression of VEGFR-1/3 in HNC.

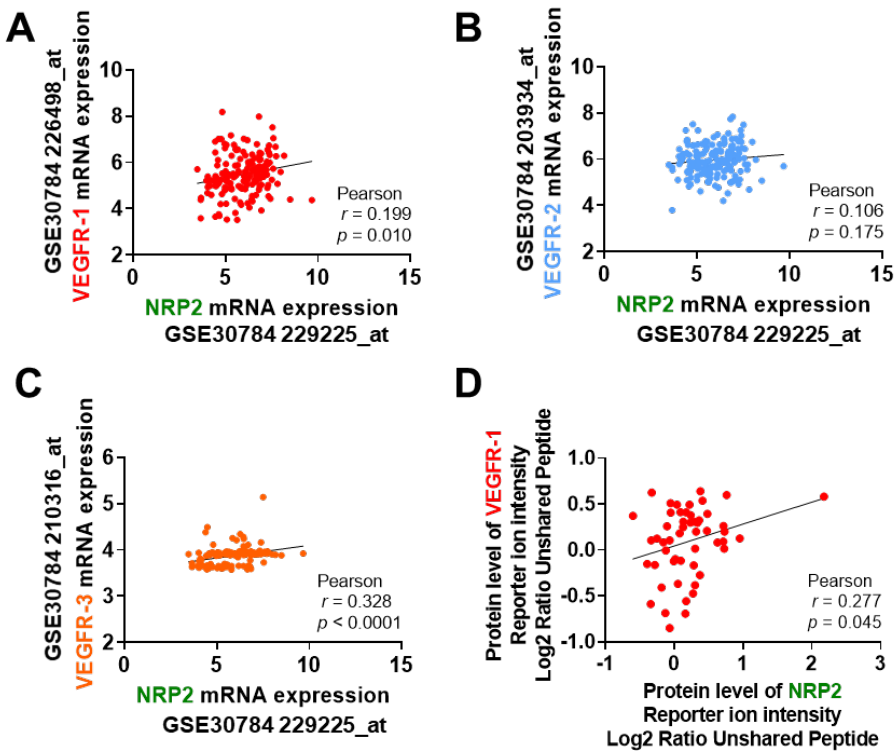

Figure 23. Correlations between NRP2 and VEGFRs expression levels. (A–C) Correlations between NRP2 and VEGFR-1/2/3 mRNA levels were represented using GEO dataset (GSE30784). (D) A positive correlation between NRP2 and VEGFR-1 protein levels was represented using CPTAC.

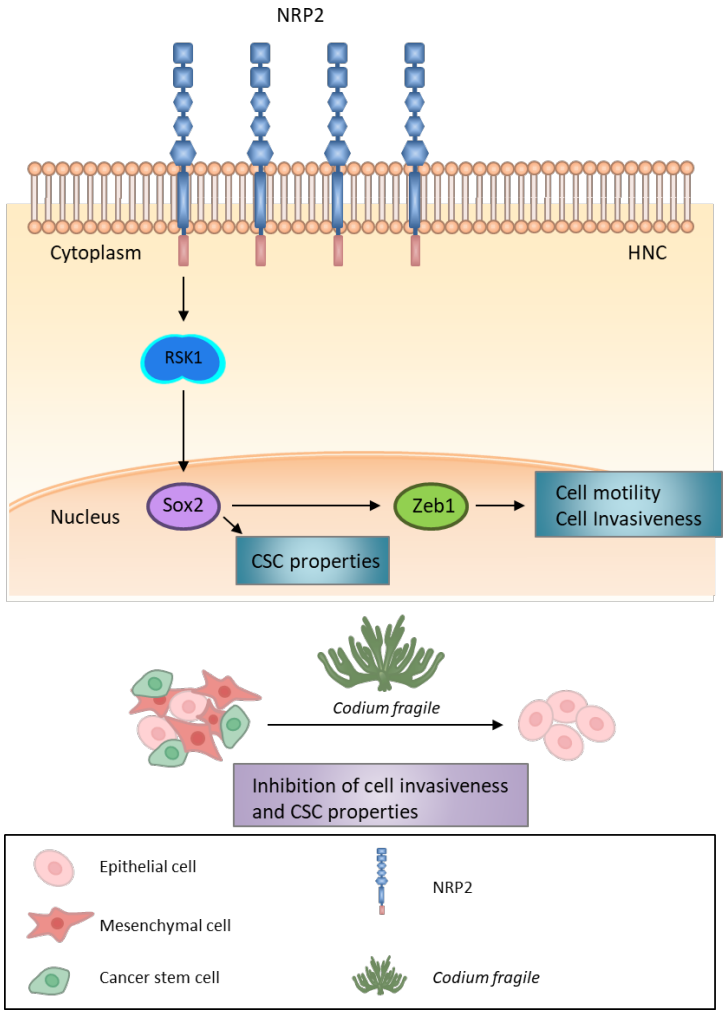

Figure 24. Schematic model. In HNC, oncogenic NRP2 regulates cell motility, invasiveness, and CSC properties through RSK1/Sox2/Zeb1 axis. MECF can inhibit these metastatic events by targeting NRP2 onco-pathway, suggesting that MECF is a prospective candidate for natural medicines to suppress metastatic potential in HNC.

Ⅳ. Discussion

In this study, I demonstrated the pivotal functional role of NRP2 that acts as a driver of metastatic events and the corresponding mechanism to exert the NRP2/RSK1/Sox2 axis in HNC cell lines. It also revealed that MECF targeting NRP2 could regulate HNC cell lines at the same signaling axis, suggesting the possibility of a promising anticancer drug for HNC patients.

Many other studies have reported the overexpression of NRP2 in different tumors including epithelial ovarian carcinoma, non-small cell lung cancer, and OSCC suggesting a potential oncogenic molecule in cancer progression (Grandclement and Borg, 2011, Osada et al, 2006, Kawakami et al, 2002, Liu et al, 2017). My results demonstrated that the expression level of NRP2 in various human cancer types was higher than normal *in silico* analysis (Figure 1A) and the mRNA and protein expressions of NRP2 in HNC were significantly higher than normal (Figure 2). The results also showed that the protein expression of NRP2 was predominantly higher in various HNC cell lines compared to HOK (Figure 6A). NRP1 is also

highly expressed in various cancer types, such as pancreatic (Wey et al, 2005), lung (Jubb et al, 2012), breast (Stephenson et al, 2002), and prostate cancer (Wey et al, 2005). NRP1 plays a crucial role in cancer progression and angiogenesis through VEGFR2/PI3K/Akt signaling (Hong et al, 2007). On the contrary, I found that the mRNA or protein expressions of NRP1 in HNC were shown little change or were lower than normal and that the correlation between NRP1 and NRP2 protein levels was insignificant *in silico* analysis (Figure 3). These indicate that NRP2, but not NRP1, is predominantly expressed in HNC and may have an important role in HNC development.

Most studies primarily reported that NRP2, as a co-receptor, contributes to metastasis, angiogenesis, and lymphangiogenesis by directly interacting with tyrosine kinase VEGFRs in cancer (Karpanen et al, 2006, Sulpice et al, 2008). Sanchez-Carbayo et al. determined that NRP2 with VEGFR-1 are co-localized in bladder urothelial and ganglia cells, which is associated with advanced tumor stage and grade in bladder cancer (Sanchez-Carbayo et al, 2003). NRP2 plays a role in lymphangiogenesis by interacting with VEGFR-2/3 in endothelial cells (Karpanen et al, 2006). NRP2 is also co-

expressed with VEGFR-3 and its interaction induced lymph vascular development and LNM in mouse models (Lohela et al, 2009). Disruption of the interaction between NRP2 and VEGFR-1 reduced cell motility, invasiveness, anchorage-independent growth, and survival of tumor cells in colorectal cancer cells (Gray et al, 2008). In another concept, a few results showed that VEGF/NRP2 has the ability to mediate signaling independently of VEGFR. Elaimy et al. demonstrated autocrine VEGF/NRP2 signaling to sustain the activation of TAZ induces CSC properties without associating VEGFR (Elaimy et al, 2018). They also reported that autocrine VEGF/NRP2 signaling is mediated by YAP/TAZ by regulating Rad51 in DNA repair (Elaimy et al, 2019). To estimate how NRP2 exerts its functional role in HNC, *in silico* analysis between NRP2 and VEGFRs was performed. My results showed that the mRNA expression levels of VEGFR-1/3 in OSCC and the protein expression levels of VEGFR-1 were positively correlated with NRP2 in HNC using GEO dataset (GSE30784) or CPTAC, respectively (Figure 23A, 23C-D). In fact, NRP2 interacts with VEGFR-2 in small intestinal neuroendocrine tumors progression and regulates VEGFR-2 transcription by

regulating the nuclear translocation of VEGFR-2 (Bollard et al, 2019). However, their correlation between NRP2 and VEGFR-2 has still not been revealed in SCC. My result showed that the mRNA expression levels of NRP2 are not associated with VEGFR-2 in GEO dataset (Figure 23B). These suggest that enhancing metastatic traits by NRP2 in HNC may be related to the expression of VEGFR-1/3.

According to my results, the high intensity of NRP2 was significantly associated with positive LNM (N2) and was also linked with poor prognosis and survival rate (Figure 4 and Figure 5). I also *in vitro* verified that NRP2 suppressed cell proliferation, motility, and invasiveness in NRP2 knockdown stable HNC cell lines (Figure 7 and 8). On the contrary, the result showed the opposite effect in NRP2 O/E stable HSC-2 cell lines (Figure 16 and 17A). The previous study has demonstrated that the expression of NRP2 in salivary adenoid cystic carcinoma, approximately 10 % of all epithelial salivary tumors, was correlated with vascular invasion, and metastasis (Cai et al, 2010). Characteristics of OSCC are aggressive and occur easily regional metastasis and are diagnosed with positive LNM in almost 50 % of the patient' s neck (Fang et al, 2019, Zhang et al, 2021).

Thus, it raises a possibility that main function of NRP2 in HNC may be related with metastasis.

EMT is a dynamic and transient process that promotes cancer cell progression and invasion by causing dysfunction of cell-to-cell adhesions and junctions and altering epithelial phenotype in the surrounding tumor microenvironment (Kalluri and Weinberg, 2009). I found that the morphology of NRP2 knockdown stable cell lines became less invasive indicating that the mesenchymal-epithelial transition which is the reverse EMT process underwent by knocking down NRP2 (Figure 8A). I also demonstrated that the expression of Zeb1 and migratory and invasive abilities were regulated when NRP2 was knockdown or overexpressed in HNC, suggesting that the key EMT marker regulated by NRP2 signaling was Zeb1 in HNC cell lines (Figure 18). Zeb1 is a well-known EMT-induced transcription factor and is stimulated by TGF-β to upregulate NRP2 (Nasarre et al, 2013). Zeb1 acts as a transcriptional repressor in the E-cadherin promoter and loss of E-cadherin by Zeb1 is associated with increasing metastatic traits and poor clinical prognosis (Sanchez-Tillo et al, 2010). Contrary to my expectations, the results showed

that the protein expression level of E-cadherin in NRP2 knockdown stable HSC-4 and FaDu cell lines increased compared with scramble cell lines (Figure 18A), whereas its expression was inconsistent in the rest of the results (Figure 18B-D). These results indicate that E-cadherin is not necessarily regulated by the expression of Zeb1. MA Nieto., et al. suggested the concept of partial EMTs which can occur by sharing epithelial and mesenchymal traits to control epithelial plasticity in cancer cells (Nieto, 2013). Other group also demonstrated that downregulation of E-cadherin is not essentially associated with the EMT program (Navarro et al, 1993). These suggest that NRP2 signaling may be sufficient to play a role in the metastasis of HNC by regulating only the Zeb1 protein without regulating E-cadherin.

Cells with self-renewal capacity among cancer cells are defined as CSC. It is distributed in multiple tumor cells and promotes tumor growth by causing abnormal differentiation (Han et al, 2020). Stemness-associated markers including Sox2, Nanog, and Oct4, which are involved in the maintenance of embryonic stem cell stemness, recently have demonstrated regulation of tumorigenesis

and metastasis (Boumahdi et al, 2014). My findings demonstrated that Sox2 is a downstream regulatory molecule of NRP2 by showing that the expression level of Sox2 was downregulated in NRP2 knockdown stable HNC cell lines (Figure 9). I also confirmed that the knockdown of Sox2 inhibited migratory and invasive abilities in HNC cell lines (Figure 10). The transcription factor Sox2 is one of the SRY-related high-mobility-group box family (Schepers et al, 2002). It is expressed in a diversity of stem cells and genetically amplified in various cancers, including tongue SCC (Sun et al, 2012), lung SCC (Ferone et al, 2016), breast cancer (Leis et al, 2012), and colorectal cancer (Lundberg et al, 2016), and thus promotes cell proliferation, invasion, and metastasis (Ren et al, 2016). Han. X., et al. demonstrated that knockdown of Sox2 decreased cell mobility and invasive abilities *in vitro* and reduced metastasis *in vivo* by inducing an EMT in colorectal cancer (Alonso et al, 2011). Lu Y. X., et al. demonstrated that the translation of EMT-activator, Zeb1 was inhibited by miR-200c, which regulates the expression of Sox2 through a negative-feedback loop in colorectal cancer (Lu et al, 2014). These concepts considerably supported my findings that

alterations in cell motility and invasiveness might be linked with the Zeb1 by regulating Sox2 in HNC. Nanog and Oct4, other biomarkers of CSCs, are important regulators of early development, maintain the pluripotency of embryonic stem cells (Boyer et al, 2005), and regulate cancer progression (Ezeh et al, 2005). Nanog induced EMT initiating process by increasing the expression of N-cadherin during cancer progression (Xu et al, 2022, Qin et al, 2017) and Oct4 is associated with invasion of HNC by regulating Slug (Koo et al, 2015) meaning that these two molecules may be related with cancer invasion and progression by regulating EMT. My results except for the experiment for the treatment of MECF showed that the expression of Nanog was significantly regulated, whereas the expression of Oct4 was not significantly altered (Figure 10A, 14A, 16B and 21A). Rodda, D.J., et al. reported that Sox2 and Oct4 are upstream transcription factors of Nanog and regulate the expression level of the corresponding gene by interacting with the Nanog promoter (Rodda et al, 2005). Based on my results, it seems that Sox2 and Nanog together modulate CSC properties. Several studies have applied serial subculturing of *in vitro* tumor spheres formation

to evaluate their self-renewal capacity (Kreso and Dick, 2014, Calvet et al, 2014). My results showed that tumor sphere-forming efficiency was decreased in NRP2 knockdown stable HNC cell lines (Figure 11B) and was reversely increased in NRP2 O/E stable HSC-2 cell lines (Figure 17C). These suggest that the downregulation of Sox2 suppressed the migratory and invasive potential of HNC by regulating Zeb1 and also reduced CSC properties along with Nanog.

Ras-mitogen-activated protein kinase (MAPK) is generally involved in cell proliferation, survival, and differentiation by binding growth factors such as TGF-α to tyrosine kinase receptors and these signaling components cause mutations or overexpression in human cancer (Roberts and Der, 2007). The RSKs are downstream of the MAPK kinase and have four types of isoforms (RSK 1-4). They commonly have activation loop sequences that bind directly to ERK for phosphorylation (Anjum and Blenis, 2008). In this study, in accordance with 1,358 protein profiling, only RSK1 was significantly regulated by NRP2 (Figure 12). Blocking RSK1 using BI-D1870 reduced the expression of Sox2 and then inhibited migratory, invasive, and tumor-sphere forming abilities in HNC cell lines

(Figure 13 – 15). Consistent with my results, Li, M.Y., et al. also showed that combination treatment of BI-D1870 and radiotherapy suppressed CSC properties and enabled to overcome radio-resistance in esophageal SCC (Li et al, 2020). These results indicate that RSK1 is a main route that links with Sox2 through NRP2 signaling in HNC.

Algae constitute more than 15,000 biologically active polysaccharides such as carrageenan, alginic acid, fucoidan, laminaran, and porphyrin. These active compounds of primary metabolisms make essential contributions to the survival, growth, reproduction, and defense of the organism itself and the secondary metabolites also contributed to pharmacological benefits (Pomin and ProQuest, 2012, Cabrita et al, 2010). Despite many relevant studies of marine natural compounds, no identified natural compounds targeting NRP2 for anti-metastatic effects have been identified so far. I found that MECF has the anti-metastatic effect by targeting NRP2 without influencing cell viability (Figure 19). Interestingly, MECF had an anti-invasive ability in FaDu cells, but the migratory ability was not changed (Figure 20). Several previous studies have

demonstrated that cell migration is just movement from one location to another (Trepat et al, 2012), whereas cell invasion is the crucial motile ability that infiltrates neighboring tissues by degrading the extracellular matrix (Sibley et al, 1994). Recently, Hua X et al.(Hua et al, 2020) Cheliensisin A remarkably inhibited only the invasive ability of human invasive bladder cancer cells through downregulation of Sox2 protein expression, but not migratory ability. Consistent with my result, it is possible to affect only invasion ability by MECF without affecting migration. I also demonstrated that MECF downregulated the expression levels of all molecules along the NRP2/RSK1/Sox2 axis and suppressed cell invasiveness by regulating Zeb1 (Figure 21), and also reduced the tumor-sphere forming efficiency by significantly decreasing the expression of Nanog and Oct4 (Figure 22). These results suggested that MECF targeting NRP2 possesses remarkable anti-metastatic activity in HNC.

Ⅴ. Conclusions

In summary, I have mechanically demonstrated that previously unknown signaling of NRP2 is involved in the metastatic traits of HNC such as cell migration, invasiveness, and CSC properties. NRP2 is overexpressed in HNC tissues and cell lines and is associated with the tumor size, LNM, tumor stage, and survival rate and MECF targeting NRP2 contributes to overcoming metastasis. These suggest that NRP2 might be a valuable therapeutic target and a potential diagnostic marker for HNC and MECF might be a prospective natural pharmaceutical agent in HNC patients (Figure 24).

Ⅵ. References

AKAGI, K., IKEDA, Y., MIYAZAKI, M., ABE, T., KINOSHITA, J., MAEHARA, Y. & SUGIMACHI, K. Vascular endothelial growth factor-C (VEGF-C) expression in human colorectal cancer tissues. *Br J Cancer*. Oct 2000;83(7):887-891. doi:10.1054/bjoc.2000.1396

ALONSO, M. M., DIEZ-VALLE, R., MANTEROLA, L., RUBIO, A., LIU, D., CORTES-SANTIAGO, N., URQUIZA, L., JAUREGI, P., LOPEZ DE MUNAIN, A., SAMPRON, N., ARAMBURU, A., TEJADA-SOLIS, S., VICENTE, C., ODERO, M. D., BANDRES, E., GARCIA-FONCILLAS, J., IDOATE, M. A., LANG, F. F., FUEYO, J. & GOMEZ-MANZANO, C. Genetic and epigenetic modifications of Sox2 contribute to the invasive phenotype of malignant gliomas. *PLoS One*. 2011;6(11):e26740. doi:10.1371/journal.pone.0026740

AMIN, M. B., GREENE, F. L., EDGE, S. B., COMPTON, C. C., GERSHENWALD, J. E., BROOKLAND, R. K., MEYER, L., GRESS, D. M., BYRD, D. R. & WINCHESTER, D. P. The Eighth Edition AJCC Cancer Staging Manual: Continuing to build a bridge from a population-based to a more "personalized" approach to cancer staging. *CA Cancer J Clin*. Mar 2017;67(2):93-99. doi:10.3322/caac.21388

ANJUM, R. & BLENIS, J. The RSK family of kinases: emerging roles in cellular signalling. *Nat Rev Mol Cell Biol*. Oct 2008;9(10):747-758. doi:10.1038/nrm2509

BARRETT, T., WILHITE, S. E., LEDOUX, P., EVANGELISTA, C., KIM, I. F., TOMASHEVSKY, M., MARSHALL, K. A., PHILLIPPY, K. H., SHERMAN, P. M., HOLKO, M., YEFANOV, A., LEE, H., ZHANG, N., ROBERTSON, C. L., SEROVA, N., DAVIS, S. & SOBOLEVA, A. NCBI GEO: archive for functional genomics data sets--update. *Nucleic Acids Res*. Jan 2013;41(Database issue):D991-995. doi:10.1093/nar/gks1193

BHARDWAJ, M., MANI, S., MALARVIZHI, R., SALI, V. K. & VASANTHI, H. R. Immunomodulatory activity of brown algae Turbinaria ornata derived sulfated polysaccharide on LPS induced systemic inflammation. *Phytomedicine*. Aug 2021;89:153615. doi:10.1016/j.phymed.2021.153615

BIELENBERG, D. R., PETTAWAY, C. A., TAKASHIMA, S. & KLAGSBRUN, M. Neuropilins in neoplasms: expression, regulation, and function. *Exp Cell Res*. Mar 10 2006;312(5):584-593. doi:10.1016/j.yexcr.2005.11.024

BOLLARD, J., PATTE, C., RADKOVA, K., MASSOMA, P., CHARDON, L., VALANTIN, J., GADOT, N., GODDARD, I., VERCHERAT, C.,

HERVIEU, V., GOUYSSE, G., PONCET, G., SCOAZEC, J. Y., WALTER, T. & ROCHE, C. Neuropilin-2 contributes to tumor progression in preclinical models of small intestinal neuroendocrine tumors. *J Pathol*. Nov 2019;249(3):343-355. doi:10.1002/path.5321

BOROWICZ, S., VAN SCOYK, M., AVASARALA, S., KARUPPUSAMY RATHINAM, M. K., TAULER, J., BIKKAVILLI, R. K. & WINN, R. A. The soft agar colony formation assay. *J Vis Exp*. Oct 27 2014;(92):e51998. doi:10.3791/51998

BOUMAHDI, S., DRIESSENS, G., LAPOUGE, G., RORIVE, S., NASSAR, D., LE MERCIER, M., DELATTE, B., CAAUWE, A., LENGLEZ, S., NKUSI, E., BROHEE, S., SALMON, I., DUBOIS, C., DEL MARMOL, V., FUKS, F., BECK, B. & BLANPAIN, C. SOX2 controls tumour initiation and cancer stem-cell functions in squamous-cell carcinoma. *Nature*. Jul 10 2014;511(7508):246-250. doi:10.1038/nature13305

BOYER, L. A., LEE, T. I., COLE, M. F., JOHNSTONE, S. E., LEVINE, S. S., ZUCKER, J. P., GUENTHER, M. G., KUMAR, R. M., MURRAY, H. L., JENNER, R. G., GIFFORD, D. K., MELTON, D. A., JAENISCH, R. & YOUNG, R. A. Core transcriptional regulatory circuitry in human embryonic stem cells. *Cell*. Sep 23 2005;122(6):947-956.

doi:10.1016/j.cell.2005.08.020

CABRITA, M. T., VALE, C. & RAUTER, A. P. Halogenated compounds from marine algae. *Mar Drugs*. Aug 9 2010;8(8):2301-2317. doi:10.3390/md8082301

CAI, Y., WANG, R., ZHAO, Y. F., JIA, J., SUN, Z. J. & CHEN, X. M. Expression of Neuropilin-2 in salivary adenoid cystic carcinoma: its implication in tumor progression and angiogenesis. *Pathol Res Pract*. Dec 15 2010;206(12):793-799. doi:10.1016/j.prp.2010.08.001

CALVET, C. Y., ANDRE, F. M. & MIR, L. M. The culture of cancer cell lines as tumorspheres does not systematically result in cancer stem cell enrichment. *PLoS One*. 2014;9(2):e89644. doi:10.1371/journal.pone.0089644

CERAMI, E., GAO, J., DOGRUSOZ, U., GROSS, B. E., SUMER, S. O., AKSOY, B. A., JACOBSEN, A., BYRNE, C. J., HEUER, M. L., LARSSON, E., ANTIPIN, Y., REVA, B., GOLDBERG, A. P., SANDER, C. & SCHULTZ, N. The cBio cancer genomics portal: an open platform for exploring multidimensional cancer genomics data. *Cancer Discov*. May 2012;2(5):401-404. doi:10.1158/2159-8290.CD-12-0095

CHANDRASHEKAR, D. S., BASHEL, B., BALASUBRAMANYA, S. A. H., CREIGHTON, C. J., PONCE-RODRIGUEZ, I., CHAKRAVARTHI, B. & VARAMBALLY, S. UALCAN: A Portal for Facilitating Tumor

Subgroup Gene Expression and Survival Analyses. *Neoplasia*. Aug 2017;19(8):649-658. doi:10.1016/j.neo.2017.05.002

CHEN, H., CHEDOTAL, A., HE, Z., GOODMAN, C. S. & TESSIER-LAVIGNE, M. Neuropilin-2, a novel member of the neuropilin family, is a high affinity receptor for the semaphorins Sema E and Sema IV but not Sema III. *Neuron*. Sep 1997;19(3):547-559. doi:10.1016/s0896-6273(00)80371-2

CHOI, J. H., SAPKOTA, K., PARK, S. E., KIM, S. & KIM, S. J. Thrombolytic, anticoagulant and antiplatelet activities of codiase, a bi-functional fibrinolytic enzyme from Codium fragile. *Biochimie*. Jun 2013;95(6):1266-1277. doi:10.1016/j.biochi.2013.01.023

CHOW, L. Q. M. Head and Neck Cancer. *N Engl J Med*. Jan 2 2020;382(1):60-72. doi:10.1056/NEJMra1715715

CLARKE, M. F., DICK, J. E., DIRKS, P. B., EAVES, C. J., JAMIESON, C. H., JONES, D. L., VISVADER, J., WEISSMAN, I. L. & WAHL, G. M. Cancer stem cells--perspectives on current status and future directions: AACR Workshop on cancer stem cells. *Cancer Res*. Oct 1 2006;66(19):9339-9344. doi:10.1158/0008-5472.CAN-06-3126

COHEN, N., FEDEWA, S. & CHEN, A. Y. Epidemiology and Demographics of the Head and Neck Cancer Population. *Oral Maxillofac Surg Clin North Am*. Nov 2018;30(4):381-395.

doi:10.1016/j.coms.2018.06.001

DILSHARA, M. G., JAYASOORIYA, R. G., KANG, C. H., CHOI, Y. H. & KIM, G. Y. Methanol extract of Codium fragile inhibits tumor necrosis factor-alpha-induced matrix metalloproteinase-9 and invasiveness of MDA-MB-231 cells by suppressing nuclear factor-kappaB activation. *Asian Pac J Trop Med*. Jun 2016;9(6):535-541. doi:10.1016/j.apjtm.2016.04.010

DONIA, M. & HAMANN, M. T. Marine natural products and their potential applications as anti-infective agents. *Lancet Infect Dis*. Jun 2003;3(6):338-348. doi:10.1016/s1473-3099(03)00655-8

EL-NAGGAR, A. K. Editor's perspective on the 4th edition of the WHO head and neck tumor classification. *Journal of the Egyptian National Cancer Institute*. Jun 2017;29(2):65-66. doi:10.1016/j.jnci.2017.03.003

ELAIMY, A. L., AMANTE, J. J., ZHU, L. J., WANG, M., WALMSLEY, C. S., FITZGERALD, T. J., GOEL, H. L. & MERCURIO, A. M. The VEGF receptor neuropilin 2 promotes homologous recombination by stimulating YAP/TAZ-mediated Rad51 expression. *Proc Natl Acad Sci U S A*. Jul 9 2019;116(28):14174-14180. doi:10.1073/pnas.1821194116

ELAIMY, A. L., GURU, S., CHANG, C., OU, J., AMANTE, J. J., ZHU, L. J.,

GOEL, H. L. & MERCURIO, A. M. VEGF-neuropilin-2 signaling promotes stem-like traits in breast cancer cells by TAZ-mediated repression of the Rac GAP beta2-chimaerin. *Sci Signal*. May 1 2018;11(528)doi:10.1126/scisignal.aao6897

EZEH, U. I., TUREK, P. J., REIJO, R. A. & CLARK, A. T. Human embryonic stem cell genes OCT4, NANOG, STELLAR, and GDF3 are expressed in both seminoma and breast carcinoma. *Cancer*. Nov 15 2005;104(10):2255-2265. doi:10.1002/cncr.21432

FANG, Q., LI, P., QI, J., LUO, R., CHEN, D. & ZHANG, X. Value of lingual lymph node metastasis in patients with squamous cell carcinoma of the tongue. *Laryngoscope*. Nov 2019;129(11):2527-2530. doi:10.1002/lary.27927

FERONE, G., SONG, J. Y., SUTHERLAND, K. D., BHASKARAN, R., MONKHORST, K., LAMBOOIJ, J. P., PROOST, N., GARGIULO, G. & BERNS, A. SOX2 Is the Determining Oncogenic Switch in Promoting Lung Squamous Cell Carcinoma from Different Cells of Origin. *Cancer Cell*. Oct 10 2016;30(4):519-532. doi:10.1016/j.ccell.2016.09.001

GANESAN, P., MATSUBARA, K., OHKUBO, T., TANAKA, Y., NODA, K., SUGAWARA, T. & HIRATA, T. Anti-angiogenic effect of siphonaxanthin from green alga, Codium fragile. *Phytomedicine*. Dec

1 2010;17(14):1140-1144. doi:10.1016/j.phymed.2010.05.005

GOEL, H. L., PURSELL, B., CHANG, C., SHAW, L. M., MAO, J., SIMIN, K., KUMAR, P., VANDER KOOI, C. W., SHULTZ, L. D., GREINER, D. L., NORUM, J. H., TOFTGARD, R., KUPERWASSER, C. & MERCURIO, A. M. GLI1 regulates a novel neuropilin-2/alpha6beta1 integrin based autocrine pathway that contributes to breast cancer initiation. *EMBO Mol Med.* Apr 2013;5(4):488-508. doi:10.1002/emmm.201202078

GRANDCLEMENT, C. & BORG, C. Neuropilins: a new target for cancer therapy. *Cancers (Basel).* Apr 8 2011;3(2):1899-1928. doi:10.3390/cancers3021899

GRANDCLEMENT, C., PALLANDRE, J. R., VALMARY DEGANO, S., VIEL, E., BOUARD, A., BALLAND, J., REMY-MARTIN, J. P., SIMON, B., ROULEAU, A., BOIREAU, W., KLAGSBRUN, M., FERRAND, C. & BORG, C. Neuropilin-2 expression promotes TGF-beta1-mediated epithelial to mesenchymal transition in colorectal cancer cells. *PLoS One.* 2011;6(7):e20444. doi:10.1371/journal.pone.0020444

GRAY, M. J., VAN BUREN, G., DALLAS, N. A., XIA, L., WANG, X., YANG, A. D., SOMCIO, R. J., LIN, Y. G., LIM, S., FAN, F., MANGALA, L. S., ARUMUGAM, T., LOGSDON, C. D., LOPEZ-BERESTEIN, G., SOOD, A. K. & ELLIS, L. M. Therapeutic targeting of neuropilin-2 on

colorectal carcinoma cells implanted in the murine liver. *J Natl Cancer Inst*. Jan 16 2008;100(2):109-120. doi:10.1093/jnci/djm279

HAN, J., WON, M., KIM, J. H., JUNG, E., MIN, K., JANGILI, P. & KIM, J. S. Cancer stem cell-targeted bio-imaging and chemotherapeutic perspective. *Chem Soc Rev*. Nov 21 2020;49(22):7856-7878. doi:10.1039/d0cs00379d

HARISINGHANI, M. G. & SPRINGERLINK 2013. *Atlas of Lymph Node Anatomy,* New York, NY, Springer New York : Imprint: Springer.

HONG, T. M., CHEN, Y. L., WU, Y. Y., YUAN, A., CHAO, Y. C., CHUNG, Y. C., WU, M. H., YANG, S. C., PAN, S. H., SHIH, J. Y., CHAN, W. K. & YANG, P. C. Targeting neuropilin 1 as an antitumor strategy in lung cancer. *Clin Cancer Res*. Aug 15 2007;13(16):4759-4768. doi:10.1158/1078-0432.CCR-07-0001

HU, Y., CHEN, J., HU, G., YU, J., ZHU, X., LIN, Y., CHEN, S. & YUAN, J. Statistical research on the bioactivity of new marine natural products discovered during the 28 years from 1985 to 2012. *Mar Drugs*. Jan 7 2015;13(1):202-221. doi:10.3390/md13010202

HUA, X., HUANG, M., DENG, X., XU, J., LUO, Y., XIE, Q., XU, J., TIAN, Z., LI, J., ZHU, J., HUANG, C., ZHAO, Q. S., HUANG, H. & HUANG, C. The inhibitory effect of compound ChlA-F on human bladder cancer cell invasion can be attributed to its blockage of SOX2 protein. *Cell*

Death Differ. Feb 2020;27(2):632-645. doi:10.1038/s41418-019-0377-7

HUANG, C., CHEN, L., SAVAGE, S. R., EGUEZ, R. V., DOU, Y., LI, Y., DA VEIGA LEPREVOST, F., JAEHNIG, E. J., LEI, J. T., WEN, B., SCHNAUBELT, M., KRUG, K., SONG, X., CIESLIK, M., CHANG, H. Y., WYCZALKOWSKI, M. A., LI, K., COLAPRICO, A., LI, Q. K., CLARK, D. J., HU, Y., CAO, L., PAN, J., WANG, Y., CHO, K. C., SHI, Z., LIAO, Y., JIANG, W., ANURAG, M., JI, J., YOO, S., ZHOU, D. C., LIANG, W. W., WENDL, M., VATS, P., CARR, S. A., MANI, D. R., ZHANG, Z., QIAN, J., CHEN, X. S., PICO, A. R., WANG, P., CHINNAIYAN, A. M., KETCHUM, K. A., KINSINGER, C. R., ROBLES, A. I., AN, E., HILTKE, T., MESRI, M., THIAGARAJAN, M., WEAVER, A. M., SIKORA, A. G., LUBINSKI, J., WIERZBICKA, M., WIZNEROWICZ, M., SATPATHY, S., GILLETTE, M. A., MILES, G., ELLIS, M. J., OMENN, G. S., RODRIGUEZ, H., BOJA, E. S., DHANASEKARAN, S. M., DING, L., NESVIZHSKII, A. I., EL-NAGGAR, A. K., CHAN, D. W., ZHANG, H., ZHANG, B. & CLINICAL PROTEOMIC TUMOR ANALYSIS, C. Proteogenomic insights into the biology and treatment of HPV-negative head and neck squamous cell carcinoma. *Cancer Cell*. Mar 8 2021;39(3):361-379 e316. doi:10.1016/j.ccell.2020.12.007

JUBB, A. M., STRICKLAND, L. A., LIU, S. D., MAK, J., SCHMIDT, M. & KOEPPEN, H. Neuropilin-1 expression in cancer and development. *J Pathol*. Jan 2012;226(1):50-60. doi:10.1002/path.2989

KAJITA, T., OHTA, Y., KIMURA, K., TAMURA, M., TANAKA, Y., TSUNEZUKA, Y., ODA, M., SASAKI, T. & WATANABE, G. The expression of vascular endothelial growth factor C and its receptors in non-small cell lung cancer. *Br J Cancer*. Jul 20 2001;85(2):255-260. doi:10.1054/bjoc.2001.1882

KALLURI, R. & WEINBERG, R. A. The basics of epithelial-mesenchymal transition. *J Clin Invest*. Jun 2009;119(6):1420-1428. doi:10.1172/JCI39104

KANG, S., ELF, S., LYTHGOE, K., HITOSUGI, T., TAUNTON, J., ZHOU, W., XIONG, L., WANG, D., MULLER, S., FAN, S., SUN, S. Y., MARCUS, A. I., GU, T. L., POLAKIEWICZ, R. D., CHEN, Z. G., KHURI, F. R., SHIN, D. M. & CHEN, J. p90 ribosomal S6 kinase 2 promotes invasion and metastasis of human head and neck squamous cell carcinoma cells. *J Clin Invest*. Apr 2010;120(4):1165-1177. doi:10.1172/JCI40582

KARATZANIS, A. D., KOUDOUNARAKIS, E., PAPADAKIS, I. & VELEGRAKIS, G. Molecular pathways of lymphangiogenesis and lymph node metastasis in head and neck cancer. *Eur Arch*

Otorhinolaryngol. Mar 2012;269(3):731-737. doi:10.1007/s00405-011-1809-2

KARPANEN, T., HECKMAN, C. A., KESKITALO, S., JELTSCH, M., OLLILA, H., NEUFELD, G., TAMAGNONE, L. & ALITALO, K. Functional interaction of VEGF-C and VEGF-D with neuropilin receptors. *FASEB J*. Jul 2006;20(9):1462-1472. doi:10.1096/fj.05-5646com

KAWAKAMI, T., TOKUNAGA, T., HATANAKA, H., KIJIMA, H., YAMAZAKI, H., ABE, Y., OSAMURA, Y., INOUE, H., UEYAMA, Y. & NAKAMURA, M. Neuropilin 1 and neuropilin 2 co-expression is significantly correlated with increased vascularity and poor prognosis in nonsmall cell lung carcinoma. *Cancer*. Nov 15 2002;95(10):2196-2201. doi:10.1002/cncr.10936

KAWASAKI, T., KITSUKAWA, T., BEKKU, Y., MATSUDA, Y., SANBO, M., YAGI, T. & FUJISAWA, H. A requirement for neuropilin-1 in embryonic vessel formation. *Development*. Nov 1999;126(21):4895-4902. doi:10.1242/dev.126.21.4895

KOO, B. S., LEE, S. H., KIM, J. M., HUANG, S., KIM, S. H., RHO, Y. S., BAE, W. J., KANG, H. J., KIM, Y. S., MOON, J. H. & LIM, Y. C. Oct4 is a critical regulator of stemness in head and neck squamous carcinoma cells. *Oncogene*. Apr 30 2015;34(18):2317-2324. doi:10.1038/onc.2014.174

KRESO, A. & DICK, J. E. Evolution of the cancer stem cell model. *Cell Stem Cell*. Mar 6 2014;14(3):275-291. doi:10.1016/j.stem.2014.02.006

LEE, J. B., HAYASHI, K., MAEDA, M. & HAYASHI, T. Antiherpetic activities of sulfated polysaccharides from green algae. *Planta Med*. Sep 2004;70(9):813-817. doi:10.1055/s-2004-827228

LEE, J. B., OHTA, Y., HAYASHI, K. & HAYASHI, T. Immunostimulating effects of a sulfated galactan from Codium fragile. *Carbohydr Res*. Jul 2 2010;345(10):1452-1454. doi:10.1016/j.carres.2010.02.026

LEIS, O., EGUIARA, A., LOPEZ-ARRIBILLAGA, E., ALBERDI, M. J., HERNANDEZ-GARCIA, S., ELORRIAGA, K., PANDIELLA, A., REZOLA, R. & MARTIN, A. G. Sox2 expression in breast tumours and activation in breast cancer stem cells. *Oncogene*. Mar 15 2012;31(11):1354-1365. doi:10.1038/onc.2011.338

LI, M. Y., FAN, L. N., HAN, D. H., YU, Z., MA, J., LIU, Y. X., LI, P. F., ZHAO, D. H., CHAI, J., JIANG, L., LI, S. L., XIAO, J. J., DUAN, Q. H., YE, J., SHI, M., NIE, Y. Z., WU, K. C., LIAO, D. J., SHI, Y., WANG, Y., YAN, Q. G., GUO, S. P., BIAN, X. W., ZHU, F., ZHANG, J. & WANG, Z. Ribosomal S6 protein kinase 4 promotes radioresistance in esophageal squamous cell carcinoma. *J Clin Invest*. Aug 3 2020;130(8):4301-4319. doi:10.1172/JCI134930

LIN, Y., QI, X., LIU, H., XUE, K., XU, S. & TIAN, Z. The anti-cancer effects

of fucoidan: a review of both in vivo and in vitro investigations. *Cancer Cell Int*. 2020;20:154. doi:10.1186/s12935-020-01233-8

LIU, Y., LI, R., YIN, K., REN, G. & ZHANG, Y. The crucial role of SEMA3F in suppressing the progression of oral squamous cell carcinoma. *Cell Mol Biol Lett*. 2017;22:32. doi:10.1186/s11658-017-0064-y

LOHELA, M., BRY, M., TAMMELA, T. & ALITALO, K. VEGFs and receptors involved in angiogenesis versus lymphangiogenesis. *Curr Opin Cell Biol*. Apr 2009;21(2):154-165. doi:10.1016/j.ceb.2008.12.012

LU, Y. X., YUAN, L., XUE, X. L., ZHOU, M., LIU, Y., ZHANG, C., LI, J. P., ZHENG, L., HONG, M. & LI, X. N. Regulation of colorectal carcinoma stemness, growth, and metastasis by an miR-200c-Sox2-negative feedback loop mechanism. *Clin Cancer Res*. May 15 2014;20(10):2631-2642. doi:10.1158/1078-0432.CCR-13-2348

LUNDBERG, I. V., EDIN, S., EKLOF, V., OBERG, A., PALMQVIST, R. & WIKBERG, M. L. SOX2 expression is associated with a cancer stem cell state and down-regulation of CDX2 in colorectal cancer. *BMC Cancer*. Jul 13 2016;16:471. doi:10.1186/s12885-016-2509-5

MARUR, S. & FORASTIERE, A. A. Head and neck cancer: changing epidemiology, diagnosis, and treatment. *Mayo Clin Proc*. Apr 2008;83(4):489-501. doi:10.4065/83.4.489

NAGY, A., MUNKACSY, G. & GYORFFY, B. Pancancer survival analysis of

cancer hallmark genes. *Sci Rep*. Mar 15 2021;11(1):6047. doi:10.1038/s41598-021-84787-5

NASARRE, P., GEMMILL, R. M., POTIRON, V. A., ROCHE, J., LU, X., BARON, A. E., KORCH, C., GARRETT-MAYER, E., LAGANA, A., HOWE, P. H. & DRABKIN, H. A. Neuropilin-2 Is upregulated in lung cancer cells during TGF-beta1-induced epithelial-mesenchymal transition. *Cancer Res*. Dec 1 2013;73(23):7111-7121. doi:10.1158/0008-5472.CAN-13-1755

NAVARRO, P., LOZANO, E. & CANO, A. Expression of E- or P-cadherin is not sufficient to modify the morphology and the tumorigenic behavior of murine spindle carcinoma cells. Possible involvement of plakoglobin. *J Cell Sci*. Aug 1993;105 (Pt 4):923-934. doi:10.1242/jcs.105.4.923

NIETO, M. A. Epithelial plasticity: a common theme in embryonic and cancer cells. *Science*. Nov 8 2013;342(6159):1234850. doi:10.1126/science.1234850

NOTO, Z., YOSHIDA, T., OKABE, M., KOIKE, C., FATHY, M., TSUNO, H., TOMIHARA, K., ARAI, N., NOGUCHI, M. & NIKAIDO, T. CD44 and SSEA-4 positive cells in an oral cancer cell line HSC-4 possess cancer stem-like cell characteristics. *Oral Oncol*. Aug 2013;49(8):787-795. doi:10.1016/j.oraloncology.2013.04.012

OHTA, Y., LEE, J. B., HAYASHI, K. & HAYASHI, T. Isolation of sulfated galactan from Codium fragile and its antiviral effect. *Biol Pharm Bull*. May 2009;32(5):892-898. doi:10.1248/bpb.32.892

OSADA, R., HORIUCHI, A., KIKUCHI, N., OHIRA, S., OTA, M., KATSUYAMA, Y. & KONISHI, I. Expression of semaphorins, vascular endothelial growth factor, and their common receptor neuropilins and alleic loss of semaphorin locus in epithelial ovarian neoplasms: increased ratio of vascular endothelial growth factor to semaphorin is a poor prognostic factor in ovarian carcinomas. *Hum Pathol*. Nov 2006;37(11):1414-1425. doi:10.1016/j.humpath.2006.04.031

PELLET-MANY, C., FRANKEL, P., JIA, H. & ZACHARY, I. Neuropilins: structure, function and role in disease. *Biochem J*. Apr 15 2008;411(2):211-226. doi:10.1042/BJ20071639

POMIN, V. H. Structure-function relationship of anticoagulant and antithrombotic well-defined sulfated polysaccharides from marine invertebrates. *Adv Food Nutr Res*. 2012;65:195-209. doi:10.1016/B978-0-12-416003-3.00012-3

POMIN, V. H. & PROQUEST 2012. *Seaweed : ecology, nutrient composition and medicinal uses,* Hauppauge, N.Y, Nova Science.

PRUD'HOMME, G. J. & GLINKA, Y. Neuropilins are multifunctional

coreceptors involved in tumor initiation, growth, metastasis and immunity. *Oncotarget*. Sep 2012;3(9):921-939. doi:10.18632/oncotarget.626

QIN, S., LI, Y., CAO, X., DU, J. & HUANG, X. NANOG regulates epithelial-mesenchymal transition and chemoresistance in ovarian cancer. *Biosci Rep*. Feb 28 2017;37(1)doi:10.1042/BSR20160247

REN, Z. H., ZHANG, C. P. & JI, T. Expression of SOX2 in oral squamous cell carcinoma and the association with lymph node metastasis. *Oncol Lett*. Mar 2016;11(3):1973-1979. doi:10.3892/ol.2016.4207

RIOUX, L. E., TURGEON, S. L. & BEAULIEU, M. Effect of season on the composition of bioactive polysaccharides from the brown seaweed Saccharina longicruris. *Phytochemistry*. May 2009;70(8):1069-1075. doi:10.1016/j.phytochem.2009.04.020

ROBERTS, P. J. & DER, C. J. Targeting the Raf-MEK-ERK mitogen-activated protein kinase cascade for the treatment of cancer. *Oncogene*. May 14 2007;26(22):3291-3310. doi:10.1038/sj.onc.1210422

RODDA, D. J., CHEW, J. L., LIM, L. H., LOH, Y. H., WANG, B., NG, H. H. & ROBSON, P. Transcriptional regulation of nanog by OCT4 and SOX2. *J Biol Chem*. Jul 1 2005;280(26):24731-24737. doi:10.1074/jbc.M502573200

ROMEO, Y., ZHANG, X. & ROUX, P. P. Regulation and function of the RSK family of protein kinases. *Biochem J.* Jan 15 2012;441(2):553-569. doi:10.1042/BJ20110289

SALVEN, P., LYMBOUSSAKI, A., HEIKKILA, P., JAASKELA-SAARI, H., ENHOLM, B., AASE, K., VON EULER, G., ERIKSSON, U., ALITALO, K. & JOENSUU, H. Vascular endothelial growth factors VEGF-B and VEGF-C are expressed in human tumors. *Am J Pathol.* Jul 1998;153(1):103-108. doi:10.1016/S0002-9440(10)65550-2

SANCHEZ-CARBAYO, M., SOCCI, N. D., LOZANO, J. J., LI, W., CHARYTONOWICZ, E., BELBIN, T. J., PRYSTOWSKY, M. B., ORTIZ, A. R., CHILDS, G. & CORDON-CARDO, C. Gene discovery in bladder cancer progression using cDNA microarrays. *Am J Pathol.* Aug 2003;163(2):505-516. doi:10.1016/S0002-9440(10)63679-6

SANCHEZ-TILLO, E., LAZARO, A., TORRENT, R., CUATRECASAS, M., VAQUERO, E. C., CASTELLS, A., ENGEL, P. & POSTIGO, A. ZEB1 represses E-cadherin and induces an EMT by recruiting the SWI/SNF chromatin-remodeling protein BRG1. *Oncogene.* Jun 17 2010;29(24):3490-3500. doi:10.1038/onc.2010.102

SCHEPERS, G. E., TEASDALE, R. D. & KOOPMAN, P. Twenty pairs of sox: extent, homology, and nomenclature of the mouse and human sox transcription factor gene families. *Dev Cell.* Aug 2002;3(2):167-

170. doi:10.1016/s1534-5807(02)00223-x

SHINTANI, S., LI, C., ISHIKAWA, T., MIHARA, M., NAKASHIRO, K. & HAMAKAWA, H. Expression of vascular endothelial growth factor A, B, C, and D in oral squamous cell carcinoma. *Oral Oncol*. Jan 2004;40(1):13-20. doi:10.1016/s1368-8375(03)00127-1

SIBLEY, L. D., DOBROWOLSKI, J., MORISAKI, J. H. & HEUSER, J. E. Invasion and Intracellular Survival by Toxoplasma-Gondii. *Baillieres Clinical Infectious Diseases*. Jul 1994;1(2):245-264.

STATON, C. A., KUMAR, I., REED, M. W. & BROWN, N. J. Neuropilins in physiological and pathological angiogenesis. *J Pathol*. Jul 2007;212(3):237-248. doi:10.1002/path.2182

STEPHENSON, J. M., BANERJEE, S., SAXENA, N. K., CHERIAN, R. & BANERJEE, S. K. Neuropilin-1 is differentially expressed in myoepithelial cells and vascular smooth muscle cells in preneoplastic and neoplastic human breast: a possible marker for the progression of breast cancer. *Int J Cancer*. Oct 10 2002;101(5):409-414. doi:10.1002/ijc.10611

SULPICE, E., PLOUET, J., BERGE, M., ALLANIC, D., TOBELEM, G. & MERKULOVA-RAINON, T. Neuropilin-1 and neuropilin-2 act as coreceptors, potentiating proangiogenic activity. *Blood*. Feb 15 2008;111(4):2036-2045. doi:10.1182/blood-2007-04-084269

SUN, Y., HAN, J., LU, Y., YANG, X. & FAN, M. Biological characteristics of a cell subpopulation in tongue squamous cell carcinoma. *Oral Dis*. Mar 2012;18(2):169–177. doi:10.1111/j.1601–0825.2011.01860.x

SUNG, H., FERLAY, J., SIEGEL, R. L., LAVERSANNE, M., SOERJOMATARAM, I., JEMAL, A. & BRAY, F. Global Cancer Statistics 2020: GLOBOCAN Estimates of Incidence and Mortality Worldwide for 36 Cancers in 185 Countries. *CA Cancer J Clin*. May 2021;71(3):209–249. doi:10.3322/caac.21660

TABARSA, M., KARNJANAPRATUM, S., CHO, M., KIM, J. K. & YOU, S. Molecular characteristics and biological activities of anionic macromolecules from Codium fragile. *Int J Biol Macromol*. Aug 2013;59:1–12. doi:10.1016/j.ijbiomac.2013.04.022

THOMAS, N. V. & KIM, S. K. Beneficial effects of marine algal compounds in cosmeceuticals. *Mar Drugs*. Jan 14 2013;11(1):146–164. doi:10.3390/md11010146

TREPAT, X., CHEN, Z. & JACOBSON, K. Cell migration. *Compr Physiol*. Oct 2012;2(4):2369–2392. doi:10.1002/cphy.c110012

VERBRUGGEN, H., LELIAERT, F., MAGGS, C. A., SHIMADA, S., SCHILS, T., PROVAN, J., BOOTH, D., MURPHY, S., DE CLERCK, O., LITTLER, D. S., LITTLER, M. M. & COPPEJANS, E. Species boundaries and phylogenetic relationships within the green algal

genus Codium (Bryopsidales) based on plastid DNA sequences. *Mol Phylogenet Evol*. Jul 2007;44(1):240-254. doi:10.1016/j.ympev.2007.01.009

WELCH, D. R. & HURST, D. R. Defining the Hallmarks of Metastasis. *Cancer Res*. Jun 15 2019;79(12):3011-3027. doi:10.1158/0008-5472.CAN-19-0458

WEY, J. S., GRAY, M. J., FAN, F., BELCHEVA, A., MCCARTY, M. F., STOELTZING, O., SOMCIO, R., LIU, W., EVANS, D. B., KLAGSBRUN, M., GALLICK, G. E. & ELLIS, L. M. Overexpression of neuropilin-1 promotes constitutive MAPK signalling and chemoresistance in pancreatic cancer cells. *Br J Cancer*. Jul 25 2005;93(2):233-241. doi:10.1038/sj.bjc.6602663

WISSMANN, C. & DETMAR, M. Pathways targeting tumor lymphangiogenesis. *Clin Cancer Res*. Dec 1 2006;12(23):6865-6868. doi:10.1158/1078-0432.CCR-06-1800

WITTMANN, P., GRUBINGER, M., GROGER, C., HUBER, H., SIEGHART, W., PECK-RADOSAVLJEVIC, M. & MIKULITS, W. Neuropilin-2 induced by transforming growth factor-beta augments migration of hepatocellular carcinoma cells. *BMC Cancer*. Nov 16 2015;15:909. doi:10.1186/s12885-015-1919-0

XU, L. M., ZHANG, J., MA, Y., YUAN, Y. J., YU, H., WANG, J., CAO, X. C.,

ZHU, L. & WANG, P. MicroRNA-135 inhibits initiation of epithelial-mesenchymal transition in breast cancer by targeting ZNF217 and promoting m6A modification of NANOG. *Oncogene*. Mar 2022;41(12):1742-1751. doi:10.1038/s41388-022-02211-2

YAN, X., ZHENG, N., XIONG, X., DUAN, X., YANG, J., BIAN, H., ZHU, Z., XIONG, X. & CHEN, X. The Roles of Neuropilin 2/VEGF-C Axis in a Series of Recurrent Lymphangioma. *Eur J Pediatr Surg*. Aug 2020;30(4):337-342. doi:10.1055/s-0039-1687869

YASUOKA, H., KODAMA, R., TSUJIMOTO, M., YOSHIDOME, K., AKAMATSU, H., NAKAHARA, M., INAGAKI, M., SANKE, T. & NAKAMURA, Y. Neuropilin-2 expression in breast cancer: correlation with lymph node metastasis, poor prognosis, and regulation of CXCR4 expression. *BMC Cancer*. Jul 7 2009;9:220. doi:10.1186/1471-2407-9-220

YUAN, L., MOYON, D., PARDANAUD, L., BREANT, C., KARKKAINEN, M. J., ALITALO, K. & EICHMANN, A. Abnormal lymphatic vessel development in neuropilin 2 mutant mice. *Development*. Oct 2002;129(20):4797-4806. doi:10.1242/dev.129.20.4797

ZHANG, S., ZHANG, R., WANG, C., GONG, W., XUE, M., LIU, L. & ZHANG, Y. Central neck lymph node metastasis in oral squamous cell carcinoma at the floor of mouth. *BMC Cancer*. Mar 5 2021;21(1):225.

doi:10.1186/s12885-021-07958-7

ZHANG, Z., HELMAN, J. I. & LI, L. J. Lymphangiogenesis, lymphatic endothelial cells and lymphatic metastasis in head and neck cancer--a review of mechanisms. *Int J Oral Sci*. Mar 2010;2(1):5-14. doi:10.4248/IJOS10006

국 문 초 록

두경부 편평상피세포암에서 세포 이동성과 침습능에 대한 Neuropilin-2의 중요한 기능적 역할

안 민 혜

서울대학교 대학원

치의과학과 분자유전학 전공

지도교수 : 백 정 화

공동 지도교수 : 조 성 대

목 적

전이는 암의 특징 중 하나로, 가깝거나 먼 위치 및 기타 이차 부위로 퍼지는 과정이며 암 사망률의 주요 원인입니다. 세포 운동성과 침습성을 특징짓는 전이 사건 중 하나는 신호 전달을 통해 세포-세포 및 세포-세포 간질 간 접착을 바꿀 뿐만 아니라 상피-중간엽 전이를 통해 세포 형태를 변형시킵니다. NRP2는 주로 인간 질병에서 혈관 내피 성장인자 또는 세마포린과 같은 리간드가 결합하여 림프관 신생, 신경 발달 및 혈관 신생에 관여하는 단일 막횡단 수용체로 알려졌지만, 두경부암의 세포 운동성과 침습성에 관련한 기능은 아직 알려지지 않았습니다. 이 연구의 목적은 두경부암에서 NRP2의 중추적인 기능적 역할과 구강

편평세포암종 환자에서 림프절 전이와 임상적 연관성을 조사하는 것입니다.

방 법

두경부암에서 NRP2의 발현 패턴을 확인하기 위해 UALCAN, cBioportal, CCLE, GEO, TCGA, 그리고 CPTAC 데이터베이스를 활용하여 *in silico* 분석을 진행하였고, NRP2와 구강 편평세포암종 조직과의 임상병리학적 연관성을 확인하기 위해 면역조직 화학염색법을 수행하였습니다. 다음으로, NRP2의 신호 전달의 중추적인 기능을 밝히기 위해 안정적으로 NRP2가 녹다운 또는 과발현 된 두경부암종 세포주들에서 세포 증식 분석, 부드러운 한천 집락 형성 분석, 클론 생성 분석, 면역블로팅, 콜라겐-코팅 트랜스웰 이동 분석, 보이든-챔버 마트리젤 코팅 침입 분석, 종양 형성구 분석을 진행하였습니다. 또한, 안정적으로 NRP2가 녹다운 된 HSC-4 세포주에서 1358개의 차등적 단백질 발현량을 계층적 클러스터링 히트맵으로 표현하였습니다. 20종의 해조류 추출물을 대상으로 세포 독성분석과 면역블롯팅을 진행하여 NRP2를 표적으로 하는 후보물질을 찾고, 메탄올 추출 청각의 효능을 확인하기 위해 면역블로팅, 콜라겐-코팅 트랜스웰 이동 분석, 보이든-챔버 마트리젤 코팅 침입 분석, 종양 형성구 분석을 두경부암 세포주에서 진행하였습니다.

결 과

In silico 분석에서 NRP2의 mRNA와 유전자 카피 수와 양의 상관관계를 보였고, NRP2의 발현은 정상 조직에 비해 두경부암종 환자 조직에서 더 높다는 것을 발견했습니다. 또한, 구강 편평세포암종 환자 조직의 면역조직 화학염색 결과에서 NRP2 발현의 강도는 인접한 정상 상피보다 비정상적으로 높았으며, NRP2의 높은 발현은 림프절 전이 및 나쁜 예후와 유의하게 관련이 있음을 입증했습니다. NRP2가 안정적으로 발현이 억제 된 두경두암 세포주에서 증식, 집락 형성, 이동성 및 침습성 능력, 종양구 형성능을 억제하는 반면 NRP2가 과발현 된 경우 이러한 기능들을 증가시킨다는 것을 입증했습니다. 메커니즘적으로, RSK1이 NRP2의 다운스트림 키네이즈이며, RSK1과 phospho-RSK$^{T359/S363}$의 하향 조절은 암 줄기 세포 특성에 기여하는 Sox2를 효과적으로 감소시킨다는 것을 확인하였습니다. NRP2/RSK1/Sox2 축에 의해 조절되는 핵심 상피-중간엽 전이 마커는 Zeb1임을 확인하였습니다. 20가지 해조류 추출물 중 메탄올 추출 청각은 세포 생존율의 변화 없이 NRP2의 발현량을 감소시켰고, NRP2를 표적으로 하여 두경부암 세포주에서 NRP2/RSK1/Sox2 축을 통해 항전이 효과를 나타냄을 입증하였습니다.

결 론

이 연구는 NRP2/RSK1/Sox2 축이 상피-중간엽 전이 과정에 영향을 주어 세포 운동성 및 침습성을 발휘하고, NRP2를 표적으로 하는 메탄올 추출 청각이 인간 두경부암 세포주에서 항전이 효과에 기여할 수 있음을 시사합니다.

주요어 : 두경부암, NRP2, 전이, 상피-중간엽 전이, 청각

학 번 : 2017-23884